Journal of Sound and Vibration 509 (2021) 116223

Contents lists available at ScienceDirect

Journal of Sound and Vibration

journal homepage: www.elsevier.com/locate/jsv

Special Issue: Recent Advances in Acoustic Black Hole Research

Theoretical and experimental study of wind turbine drivetrain fault diagnosis by using torsional vibrations and modal estimation

Farid K. Moghadam*, Amir R. Nejad

Department of Marine Technology, Norwegian University of Science and Technology, Trondheim, Norway

ARTICLE INFO

Article history:
Received 29 August 2020
Revised 9 April 2021
Accepted 19 May 2021
Available online 21 May 2021

Keywords:
Drivetrain system
Torsional measurements
Modal analysis
Fault diagnosis
Sensitivity analysis
Floating wind turbines

ABSTRACT

This paper provides an analytical proof and the theoretical development of the idea of using the torsional vibration measurements for a system-level condition monitoring of the drivetrain system. The method relies on modal parameter estimation of the drivetrain system by using the torsional measurements and subsequent monitoring of the variations in the system eigenfrequencies and normal modes. Angular velocity error function extracted from encoder outputs at both input and output of drivetrain is used to estimate modal parameters including natural frequencies and damping coefficients. In the proposed condition monitoring approach, it is shown that any abnormal deviation from the reference values of the drivetrain system dynamic properties can be translated into the progression of a specific fault in the system. In order to extract the condition monitoring features, local sensitivity analysis is engaged to establish a relationship between different categories of drivetrain faults with the system dynamic properties and the amplitude of torsional response, which helps with both to identify the state of the progressive faults and to localize them. Local sensitive analysis shows that abnormal deviations in stiffness and moment of inertia due to the presence of faults result in considerable changes in natural frequencies and modal responses which can be measured and used as fault detecting features by using the proposed analytical approach. Sensitivity analysis is also employed along with the estimated modal frequency for estimation of modal damping from the amplitude of response at the natural frequencies and their subsequent use for estimation of undamped natural frequencies which are later used in the proposed condition monitoring approach. The proposed approach is computationally inexpensive and can be implemented without additional instrumentation. Two test cases, using 10 MW simulated and 1.75 MW operational drivetrains have been demonstrated.

1. Introduction

Both predictive and condition-based maintenances are proposed in the literature as potential game changers and measures which could be taken to flatten the gap between OPEX in offshore and land-based wind turbines aimed at realizing

* Corresponding author.
E-mail address: farid.k.moghadam@ntnu.no (F.K. Moghadam).

https://doi.org/10.1016/j.jsv.2021.116223

the EU 2050 plan by reduction of downtime and subsequently levelized cost of energy (LCOE) of offshore wind [1]. The motivation of this research is reducing the costly operation and maintenance of offshore turbines - more specifically the drivetrain system of floating offshore wind turbines - and improving the risk of investment by using condition-based maintenance and a subsequent reduction in downtime as one of the most influential consequences of drivetrain failures. The latter is investigated based on developing the methods which can use only the existing sensors, database, communication network and can be implemented for both fault diagnosis (as a key component of turbine operations management automation system) and offline condition monitoring (CM) purposes. The CM system is in addition to the performance monitoring, and the concept behind is monitoring of the conditions of the turbine systems with the highest risk of loss of turbine availability considering both likelihood and consequence of failures, because monitoring the condition of all systems may be economically and technologically infeasible. According to the study by Pfaffel *et al.* [2] which provides a cautious comparison on reliability characteristics of both onshore and offshore wind turbines, drivetrain system which in general includes all rotating components in power conversion system *i.e.* hub, rotor, main bearings, gearbox, generator and power converter accounts for 57% of turbine total failures and 65% of turbine total downtime. These numbers are expected to be higher in floating offshore turbines. The latter is due to more costly marine operations specially in deep waters, the larger and more expensive components, and a wider range of excitation sources due to the synergistic impacts of waves, currents and wind turbulences which call for innovative approaches to achieve a better understanding about the system dynamics and excitation sources. The focus of this research is proposing a system-level CM solution by the drivetrain modal estimation and a subsequent monitoring of abnormal variations of system modes. This goal is performed by developing a numerical model of the drivetrain as a dynamic system based on its measured torsional response and the subsequent estimation of the drivetrain torsional modes. In contrast with the other systems (*e.g.* bridges and buildings), the dynamic properties of the drivetrain do not experience a significant change over normal operations. The latter can be used to monitor any abnormality caused by faults. Therefore, variations in the drivetrain can be monitored by tracking the changes in the three modal parameters (modal frequency, modal damping and mode shape (amplitude and phase)) of the dominant modes of this system [3]. Estimation of mechanical systems dynamical characteristics is mainly based on operational modal analysis (OMA) which is challenging for drivetrain as a complex dynamical system. The latter is mainly based on translational vibration measurements [4], and the reported results in the literature show the high possibility of harmonics to be mistaken with the eigenfrequencies [3,5]. Drivetrain is a complex rotational system with different sources of external excitation and components defect frequencies. The uncertainties in the estimated modes have made available OMA techniques less-efficient for condition-based maintenance.

The current CM approaches of the wind turbine drivetrain are based on one or a combination of five categories of techniques, namely vibration analysis [6], electrical signature (current and power signals) [7], acoustic emissions analysis [8], thermography [9] and temperature analysis [10], and analysis of oil particles [11]. Today, vibration analysis is mainly based on system translational responses obtained by accelerometers (*e.g.* see [12]) with a minor attention to torsional measurements. The only commercially available drivetrain CM based on torsional measurements, is associated with the measurement of torque as the system applied load [13]. The latter is not widely used due to the matter of cost, technological limitations related to operating speed and torque ranges and shafts dimensions, intrusive nature of the torque measurement techniques, and also a lack of a standardized approach and the immature and insufficient knowledge to analyze and extract features from the torsional measurements.

Frequency response function (FRF) is a common tool which is used for modal estimation by the estimation of a system transfer function. However, the complexity of the drivetrain system and inadequacy of models in considering the internal dynamics and interactions between systems, nonlinear and synergistic impacts of different excitation sources, uncertainties in estimation of loads are some reasons which cause inexplicable harmonics and limit the application of FRF for the estimation of drivetrain dynamic properties. In this work, the operational modal analysis and fault diagnosis are based on the system torsional responses. An anterior estimation of the drivetrain loads can provide more options to the proposed algorithm. The possibility of observing drivetrain torsional natural frequencies in the torsional response is reported in [14] for different applications such as jet engine high-pressure disk, a hydro station turbine and a coal-fired power plant. The possibility of observing blade natural frequencies in drivetrain shaft torsional response and the potentials for CM of the blades is also reported in [14,15]. Suominen *et al.* [16] has reported the visibility of ship propulsion system natural frequencies in the torque measurements of the propulsion shaft due to the propeller blade contact with ice. However, these reports are based on observations on experimental studies and are not reliant on an analytical torsional model of the drivetrain systems.

The drivetrain system torsional response and the natural frequencies are proposed in the literature for detecting faults initiated by torsional sources. Patel *et al.* [17] proposes the use of angular displacement to support the lateral response to recognise the rubbing faults in the drivetrain, so that the excited torsional frequency and the amplitude of response in the natural frequency and the side bands are utilized to characterize the fault. Feng *et al.* [18] proposes the use of the measurements of torque instead of transverse vibration signals to diagnose planetary gearbox local/distributed faults, because they are free from the amplitude modulation effect caused by time variant vibration transfer paths, thus they have simpler spectral content than transverse signals. Lebold *et al.* [19] suggests monitoring the characteristic changes in torsional natural frequencies, and claims that those changes are associated with the shaft crack propagation. Kia *et al.* [20] proposes the estimated electromagnetic torque of the electrical machine as a noninvasive torsional measurement in the drivetrain to monitor the torsional stress on the components including shaft, bearings, and gearbox, and the method is used to detect a gear failure. The electromagnetic torque estimation is commonly used in electrical drives to control the electrical machine, and

implementation of the method does not need any additional sensor. Not only the drivetrain faults, but also rotor and tower excited modes may result in frequency components in the drivetrain torsional response [21]. The amplitude of response at blade edgewise and tower bending natural frequencies can provide insights about resonances in these components. The monitoring of the variations of these components frequencies is also useful for some other purposes such as ice detection in blades, and health monitoring of blades (detect root cracks within turbine blades) and tower. The idea of using angular velocity measurements for the wind turbine drivetrain fault detection was originally proposed by Nejad *et al.* [22]. The input data is provided by the encoders installed on the drivetrain for the turbine control purposes. The latter is normally accessible in both turbine and farm levels, which helps to realize CM by means of supervisory control and data acquisition (SCADA) system available measurements. Therefore, any algorithm based on those measurements can be integrated into either turbine or farm control to support the online CM of the drivetrain. Moghadam *et al.* [15] has experimentally evaluated the possibility of detecting some categories of faults in early stages by a direct utilization of torsional response, and the results of the study are compared to a conventional method based on translational vibrations obtained by accelerometers. The authors demonstrated how torsional measurements can complement the conventional approaches by providing insights on the excitation sources which are significantly influencing on the drivetrain lifetime which is useful as both a design feedback and earlier stage fault detection.

Even though the torsional response cannot directly be used for monitoring of some sort of faults, it contains the drivetrain system-level dynamic properties which can provide a near real-time modal estimation of system. From this perspective, torsional measurements are indirectly used for the drivetrain system CM purposes. For this purpose, these measurements are first used to estimate the dynamic properties of the drivetrain as a rotational system. These properties are only related to the system physical parameters and not the loading or specific operational condition, so that they can be used in the second step to monitor the variations in the drivetrain, which can be translated into a fault in case of passing a prespecified level. Moghadam *et al.* [23] has started an analytical approach to turn torsional measurements into meaningful features for fault detection purposes by specification of the analytical relationship between the system natural frequency variations and faults, and a subsequent potential for detection of system faults. The current work is dedicated to the theoretical development and simulation/experimental validation of the idea originally proposed by [23] for the modal estimation of the drivetrain by using torsional measurements, and a subsequent use of this idea to develop a method for the drivetrain system-level CM. The influence of shaft crack propagation on the torsional natural frequency was discovered by [14,24]. However, those studies lack an analytical model which describes the variations in order to establish a meaningful feature for monitoring the condition of crack. For this feature to be used as a criterion as a shaft cracking monitoring technique, a sufficient model should be provided to be able to relate the variations to the state of the fault. In addition, there are other categories of system-level faults which can also influence drivetrain torsional modes which are not considered in earlier studies.

The CM of the drivetrain at system level by using the estimated torsional natural frequencies, the normal modes, the amplitude of response in the natural frequencies and the damping of the system at natural frequencies in different operations is discussed in this paper. For this purpose, online operational measurements of the drivetrain different torsional responses including the angular velocity residual function and filtered angular velocity are employed. Drivetrain faults at system level can influence the drivetrain model parameters, so that they can be categorized into the faults that change the torsional stiffness most (*e.g.* crack in the shafts and bearing wear specially in gearbox), and faults that change mostly the inertia of the drivetrain (changes in mass balance/distrinution which can be due to *e.g.* loss of mass, wear and unbalance; and also change in the axis of rotation which can be due to *e.g.* misalignment and looseness). Regarding the relation of inertia with the square of the center of mass distance from the center of rotation, the faults which variate the center of rotation demonstrate more significant influence on the inertia and thus are more influential on the torsional dynamic properties. Among the faults that influence the inertia of the bodies in drivetrain equivalent model, there are some types which have more considerable impact on the boundary conditions between rotating and stationary elements and thus influence more drivetrain lateral responses than the torsional response (*e.g.* looseness (pedestal, shaft and bearings, coupling), [25]). The latter influences significantly lateral stiffness parameters and the lateral responses of the drivetrain, so that the detection of those faults by using the lateral response and monitoring the variations of system lateral properties could be a practical approach. Even though these faults can cause a small variation of the torsional parameters, the impact may not be significant enough for fault detection purposes. For example, a pedestal looseness may cause increased rubbing which leads to a nonlinear small increase of torsional stiffness.

By specification of the parameter in the equivalent reduced order model which will be significantly influenced by a fault, it is possible to look for the expected consequences of the associated variations of the parameter as a result of fault on the system dynamic properties, as the CM indicators. The *first category* of faults, which are detectable by the proposed CM approach, influence the torsional stiffness. Cracks in the drivetrain shafts are one of the most influential faults in this category. The initial cracks occur due to material imperfections and temperature variations in the parts of main shaft with severe stress concentration, which can grow worse under large alternating loads due to wind turbulence. To detect the shaft cracks of different relative depths, an approach based on nonlinear output FRF is proposed by [26] and experimentally tested on a simple double-disk rotor system, where the linear displacements and the bending moments are the under consideration responses but the torsional vibrations are neglected. In shaft crack faults, variation in stiffness is influenced by the crack depth and the shape of the crack front. The latter makes the detection of different types of cracks quite challenging so that a detection method suitable for one type of crack cannot be generalized to the other types. This fault does not take place as frequently as shaft unbalance or misalignment but the consequences are very high, so that the detection in very early

stages is of a high importance. If shaft cracks are not detected in early stages, the later stages of this category of faults may cause severe damage of the shaft and the occurrence of considerable secondary faults with high risk of injuries for the plant personnel. As discussed by Chatterton *et al.* [27], crack detection by using translational/axial vibrations obtained from accelerometers is challenging due to the influence of the dynamic effects caused by different components and their consequent induced vibrations. The interpretation of the data in these methods is also dependent on a deep understanding of the type of crack, its physical properties and the specific operational conditions so that the realization of an online monitoring may not be possible. The frequency and time domains analysis of accelerometers is the conventional approach to detect increased vibrations in the component-level in higher stages of a progressive fault (*e.g.* gear tooth and rolling element bearing fatigue issues). The *second category* of faults detectable by the proposed approach influence the inertia of the components in the equivalent model. In this group, misalignment and unbalance are significantly more common than the other faults. Unbalance in the rotor blades is one of the most influential and prevalent faults which can be due to different reasons *e.g.* excessive weight following a blade repair, icing, water penetration through cracks and loose material moving inside the blades. The latter causes loss in the power production. The reason for placing an emphasis on the rotor unbalance is that the highest unbalance in the drivetrain arises from the component with the highest moment of inertia which is the rotor assembly in the wind turbine drivetrain. The mass unbalance also causes additional loads on the entire structure and specially the drivetrain components so that it results in a periodic torsional (in earlier stages) and transversal (in later stages) oscillations in the wind turbine's drivetrain. It directly increases the wear of the blade on the drivetrain bearings and gears by generating asymmetrical loads. The rotor mass unbalance can be measured by monitoring its consequent variations in the drivetrain dynamic properties. As a prognostic measure, the unbalance mass can be estimated and if the detected unbalance exceeds a limit, the rotor blades should be balanced with a balancing device.

CM is mostly designed in component level, which is helping when the fault is propagated to the individual components and causes physical changes in the component level. However, the root cause of a wide range of faults are system-level issues such as unbalance, misalignment, looseness and shaft cracks. In the proposed drivetrain CM approach of this paper, it is assumed that system-level drivetrain faults (*e.g.* shaft cracks and unbalance) can reveal themselves by variations in the system stiffness and moment of inertia. Therefore, by monitoring the consequences of variations of drivetrain parameters (*i.e.* stiffness and moment of inertia matrices) in change of the drivetrain dynamic properties (*i.e.* natural frequencies, mode shapes and damping coefficients), it is possible to monitor the progress of faults. For this purpose, an analytical model of the drivetrain which represents the relationship between the system parameters and dynamic properties and a subsequent sensitivity analysis helps to realize what are the most influential system parameters/faults which can variate the drivetrain dynamic properties. *In the feature selection algorithm*, the torsional dynamical model of the drivetrain and the local sensitivity analysis are engaged. The algorithm is designed to an extent that could offer robust, fast and accurate online monitoring.

The main focus of this work are on geared drivetrain systems used for wind turbines. Based on the theoretical studies in this research work, a 3-DOF equivalent torsional model of the geared drivetrain is sufficient for detection of the drivetrain faults at a system-level, because system-level faults represent themselves mainly by changing the torsional stiffness and the moment of inertia parameters of the 3-DOF equivalent model. In the first step of the work, the proposed modal estimation approach by using the torsional measurements is presented, which is proved in the general case for a n-DOF torsional model of the drivetrain, followed by a detailed parametric proof based on 3-DOF model. As the second step of this research, the analytical relationship between the 3-DOF equivalent model parameters and drivetrain dynamic properties is established, which helps to identify the drivetrain system condition/state-of-operation by monitoring the variations in the drivetrain dynamic properties (undamped natural frequencies and normal modes) which can be estimated from the operational measurements by using the proposed modal estimation approach or the other approaches proposed by the literature. The other reason for sticking to 3-DOF model, is that the closed-form parametric expressions of the drivetrain dynamic properties as a function of equivalent model parameters can be obtained for this simplified model. Those expressions are the required inputs for the proposed fault detection approach based on monitoring the variations of the drivetrain dynamic properties. Those expressions provide quantifiable fault detection features, which are implementable in microcontrollers and can be integrated with turbine fully automated control and monitoring systems. By the increase of the order of equivalent model, more dynamic properties (higher natural frequencies which are not seen by 3-DOF model) can be employed, which can support a more detailed fault detection in the drivetrain. However, it is a little challenging for currently available modal estimation approaches to observe higher modes which appear with a low amplitude in the frequency-domain response. In other words, the real conditions for the modal estimation problem is restrictive, so that the higher eigenfrequencies of the drivetrain system, which may be excited by the input torque with a lower energy, may not be observable.

The proposed method in this paper can detect stiffness or inertia related faults by monitoring the consequences of faults on online estimated modes and amplitude of response. The method is computationally inexpensive since it relies on only few data samples and a moderate data resolution and sampling frequency. On this basis, the main contributions and novelty of this work are:

1. Analytical proof of a drivetrain modal analysis approach by using torsional measurements,
2. Introducing an analytical approach for estimation of damping coefficients of the system modes by analyzing the amplitude of torsional response error function at the natural frequencies,
3. Theoretical development and simulation/experimental validation of a drivetrain system-level health monitoring approach based on estimated modal parameters, and comparison with other methods in the literature.

The paper is organized as follows: Modal estimation by using torsional measurements is analytically elaborated in Section 2. An analytical approach for drivetrain condition monitoring by using torsional response and the estimated modes is proposed and discussed in details in Section 3. The proposed drivetrain modal estimation and condition monitoring approach are validated and compared with the approaches in the literature through simulation/experimental studies in Section 4. The paper is concluded in Section 6.

2. Operational modal analysis by using torsional measurements

2.1. Torsional natural frequency estimation theory

Drivetrain is often modelled as one-degree-of-freedom (1-DOF) rotational system in global dynamic response tools. The forced torsional vibration response of the equivalent 1-DOF damped rotational model of drivetrain influenced by the random excitation $\tau(t)$ in frequency domain and non-dimensional form can be expressed by

$$|\theta(\Omega)| = \frac{\frac{|\tau(\Omega)|}{k_t}}{\sqrt{(1-(\frac{\Omega}{\Omega_n})^2)^2 + (2\zeta_t^{\omega}(\frac{\Omega}{\Omega_n}))^2}}, \tag{1}$$

where $\theta(\Omega)$ and $\tau(\Omega)$ are the Fourier transforms of angular position and the excitation torque, respectively. Ω_n is the undamped torsional natural frequency of the system, k_t is the torsional stiffness of the shaft, and ζ_t is the torsional damping coefficient of the mode Ω_n at the operating speed ω. As it can be seen, an amplified frequency in the drivetrain torsional response can be due to a significant excitation amplitude or the vicinity of excitation frequency with natural frequencies.

Natural frequencies appear in torsional responses *e.g.* angular velocity measurements due to impulsive behavior of wind which excites those frequencies. An initial velocity applied on a system as described by Thomson *et al.*[28] can play a role as an impact which is able to excite the system torsional frequencies. In the wind turbine, the ceaseless variations of wind results in continual variations in angular velocity which is physically similar to an initial velocity applied to the system. Even though these variations in speed and subsequently torque happen in very low frequency, they can introduce considerable energy in different frequencies including the characteristic frequencies of the system. Due to the existence of damping in a real system, the measured natural frequencies from the torsional response are the damped frequencies. By filtering the shafts revolution frequencies, components defect frequencies and excitations (very low frequency due to wind, low frequency due to wave tower shadow effect, and high frequency due to generator), the drivetrain torsional natural frequencies, and some torsional induced motions due to excited edgewise rotor blade and tower bending modes are acquired. Based on a primary knowledge on the torsional frequencies for each power range, it is possible to separate the observed natural frequencies for drivetrain, blades and tower. The variations in the natural frequencies and normal modes can be used as criteria to identify some sorts of faults in the drivetrain. To estimate the damped natural frequencies, angular velocity residual/error function is proposed. The input of this method is provided by two encoders located at the high- and low-speed shafts of drivetrain, and subsequently the residual function is constructed based on the subtraction of these two signals. Some drivetrain systems are only equipped with one angular velocity measurement on the shaft, so that the implementation of the method may require an additional moderate resolution encoder to provide the sufficient inputs. The angular velocity residual function e_{tot}^{ω} from the high-speed side is expressed by

$$e_{tot}^{\omega} = \omega_{HS} - a_1 a_2 a_3 \omega_{LS}, \tag{2}$$

where ω_{HS} and ω_{LS} are the rotational speed in $\frac{rad}{s}$ obtained from the high- and low-speed encoders, respectively. a_1, a_2 and a_3 are the inverse of gear ratios of the gearbox stages. The error function main feature is cancellation of the impacts of the excitations which are transferred to the drivetrain from the housing, from the resultant torsional response. Angular displacement and acceleration are the other torsional responses of the drivetrain system which could theoretically be used similar to angular velocity to obtain the system torsional parameters. For this purpose, similar to e_{tot}^{ω}, the angular position error function e_{tot}^{θ} and the angular acceleration error function e_{tot}^{α} are defined by

$$e_{tot}^{\theta} = \theta_{HS} - a_1 a_2 a_3 \theta_{LS}, \quad e_{tot}^{\alpha} = \alpha_{HS} - a_1 a_2 a_3 \alpha_{LS}. \tag{3}$$

In particular, angular acceleration is the torsional response which has a direct relation with the applied, and contains useful information on how the applied torque interacts with the system. If acceleration or displacement is used for evaluation, the assessment criteria tends to vary with frequency, because the relation between them and velocity is proportional to frequency. The Fourier series of e_{tot}^{ω}, e_{tot}^{α} and e_{tot}^{θ} are defined by $e_{tot}^{\omega}(\Omega) = \sum_{n=-\infty}^{\infty} C_n e^{ik_n\Omega}$, $e_{tot}^{\alpha}(\Omega) = \sum_{n=-\infty}^{\infty} C_n (ik_n) e^{ik_n\Omega}$, $e_{tot}^{\theta}(\Omega) = \sum_{n=-\infty}^{\infty} C_n (ik_n)^{-1} e^{ik_n\Omega}$. Differentiation and integration are linear operations that are distributive over addition. As it can be seen, in e_{tot}^{α} compared to e_{tot}^{ω}, the amplitude of the frequency components higher than 1 Hz is magnified with the gain k_n, and the frequencies lower than 1 Hz are weakened with the same proportion. In e_{tot}^{θ} compared to e_{tot}^{ω}, the amplitude of the frequency components lower than 1 Hz is magnified with the gain k_n^{-1}, and the frequencies higher than 1 Hz are weakened with the same proportion. The 1*st* natural frequency of the drivetrain systems of the same technology decreases as the rated power increases. However, even for 10 MW wind turbine which is the biggest commercially available and even for the high-speed technologies which have lower first natural frequencies, the 1*st* torsional frequency is higher than 1 Hz [32]. Therefore, the angular acceleration error function is theoretically slightly better than the other two approaches

in highlighting the torsional frequencies. The other benefit is weakening the frequencies lower than 1 Hz which appear in the drivetrain torsional response mostly due to wind turbulence and structural motions, but do not contain any information on the drivetrain natural frequencies. However, an additional derivation operation is required to attain acceleration from the velocity measurements which increases the computational cost of this method.

A limitation with aforedescribed approach is the dependency on two encoders, because in several turbines there is only one encoder available located in the low-speed shaft. As discussed earlier, one of the significant features of the error function is cancellation of the influences of structural motions from the torsional response. The latter results in a clean signal which is able to highlight the system characteristic frequencies. Those motions are mainly influenced by wind, wave and structural resonances, and natural frequencies of structural motions and low frequency interactions between rotor, tower and support structure and have a low frequency content. Therefore, the filtered angular velocity of low-speed shaft has some potentials in highlighting the drivetrain torsional frequencies. The filtered signal $X(\Omega_{HP})$ is extracted by

$$X(\Omega) = a_1 a_2 a_3 \omega_{LS}(\Omega), \quad X(\Omega_{HP}) = X(\Omega) H(\Omega_{HP}), \tag{4}$$

where $H(\Omega_{HP})$ is the transfer function of the high-pass filter applied to the low-speed shaft encoder signal to attenuate the low frequency noises resulted wind induced low frequency motions. The performance of filtered angular velocity of low-speed shaft in highlighting the torsional frequencies compared to the different torsional response error functions is tested with both simulation and operational measurements as reported in Section 4.

In order to capture better the drivetrain dynamics at system level for the subsequent use for drivetrain fault diagnosis at system level while minimizing the computational complexity of the model, 3-DOF torsional model is offered and the performance of the model is evaluated throughout the paper. For this purpose, to evaluate the observability of natural frequencies on the torsional response error functions and the subsequent application for drivetrain CM, a 3-DOF torsional model of the damped drivetrain is engaged. The 1*st* and 2*nd* undamped natural frequencies (nonrigid modes) based on 3-DOF lumped-mass-spring model of a geared drivetrain can be calculated by the equations reported in A.1. The eigenvectors of the damped drivetrain model take complex values. By assuming damping equal to zero, the normal modes take real values which show the relative angular motion of the different inertias in the model. The closed form of two normal modes related to the two non-rigid modes of the under consideration drivetrain model which are scaled to unity length are reported in A.1.

Both undamped frequencies and normal modes are unique for the system so that any deviation of the parameters can indicate variations in the drivetrain system which can be used for fault detection. The continued discussion is dedicated on an analytical proof of the idea of observing natural frequencies from the torsional response. The theory is first presented for the general form of response obtained from the general n-DOF torsional drivetrain model. Then the possibility of observing torsional modes in amplitude of angular velocity error function based on a 3-DOF model is mathematically proven to be used in the proposed model-based fault detection approach.

Theorem 1. *Torsional natural frequencies belong to the set of extreme points of the torsional response in the frequency domain.*

Proof. The general form of the discrete multi-DOF torsional model of drivetrain with n degrees of freedom in the time domain is defined by

$$\mathbf{J}\ddot{\theta} + \mathbf{C}\dot{\theta} + \mathbf{K}\theta = T(t), \tag{5}$$

where $\mathbf{J}$, $\mathbf{C}$ and $\mathbf{K}$ are the moment of inertia, damping and stiffness matrices with the size $n \times n$. θ and T are the response and load vectors with the size $n \times 1$, where each element of these two vectors represent a time series data. The representation in frequency domain by using the frequency variable S and Laplace transform will be

$$[\mathbf{J}S^2 + \mathbf{C}S + \mathbf{K}]_{n\times n}[\Theta(S)]_{n\times 1} = T(S)_{n\times 1}. \tag{6}$$

By replacing the characteristic equation $\mathbf{J}S^2 + \mathbf{C}S + \mathbf{K}$ with $\mathbf{M}$, the frequency domain response $\Theta(S)$ will be

$$\Theta(S) = \frac{adj(\mathbf{M})}{det(\mathbf{M})} T(S), \tag{7}$$

where $adj(\mathbf{M})$ is the adjugate of $\mathbf{M}$ which is a polynomial function with the matrix variable $\mathbf{M}$. $det(\mathbf{M})$ is the determinant of the system characteristic equation. As it can be seen, the roots of the $det(\mathbf{M})$ are the extreme points of response $\Theta(S)$. However, the roots of the determinant of characteristic equation of a system are the system's eigenfrequencies. Therefore, the torsional natural frequencies of the system belong to the set of extreme points of the response. In the undamped system ($\mathbf{C} = \mathbf{0}$), the roots will be pure imaginary which represent the undamped natural frequencies Ω_n^i. In the general damped system, the roots are the damped natural frequencies Ω_d^i with the following relation with the undamped frequencies

$$\Omega_d^i = \zeta^i \Omega_n^i + j\Omega_n^i \sqrt{1 - (\zeta^i)^2} \quad i \in 1, .., n. \tag{8}$$

where ζ_i is the damping coefficient related to the mode i. The torsional natural frequencies in both cases of damped or undamped system based on the provided proof which refers to the general form of damped system are the extreme points of the response frequency domain function.

Thus, we complete the proof of Theorem 1. □

The other extreme points of $\Theta(S)$ are due to the load dynamics, the system unmodelled internal dynamics and the interactions between these two. As discussed earlier, in order to pick out the natural frequencies, other harmonics which also demonstrate themselves as other extreme points in response must be filtered. For this purpose, the response error function is engaged which is able to filter the influences of the loads transferred to the drivetrain through the structure, which is very useful specially in offshore wind turbines equipped with floating support structures which can induce a wider range of harmonics in the drivetrain response.

The typical signal for frequency domain fault detection study is the single-sided amplitude spectrum of response. In A.2, the possibility of extending the results of Theorem 1 to the amplitude of torsional response and more specifically the amplitude of angular velocity error function based on an equivalent 3-DOF model is investigated. For this purpose, the general 3-DOF damped torsional model of the geared drivetrain system is selected, and the detailed analytical proof for observing the natural frequencies in the amplitude spectrum of angular velocity error function is presented.

By replacing Ω_n from eq. (A.1) instead of $|S|$ in eq. (A.5), the amplitude of response at the two natural frequencies in the general case of a damped system has the relationship with the system parameters and loads as

$$|e^{\omega}_{tot}(\Omega^{tor}_1)| = \frac{\sqrt{|T_g(\omega 1)|^2\sqrt{FA+H+J_r^2J_{gr}^2A^2}\sqrt{A}+|T_r(\omega 1)|^2\sqrt{EA+G+J_{gr}^2J_{gn}^2A^2}\sqrt{A}}}{\sqrt[4]{A^2I^2+(J_r\sqrt{E}+c_LJ_{gr}J_{gn})^2A^3+D^2(J_r+J_{gr}+J_{gn})^2A+k_L^2k_H^2(J_r+J_{gr}+J_{gn})^2+J_r^2J_{gr}^2J_{gn}^2A^4}}, \tag{9a}$$

$$|e^{\omega}_{tot}(\Omega^{tor}_2)| = \frac{\sqrt{|T_g(\omega 2)|^2\sqrt{FB+H+J_r^2J_{gr}^2B^2}\sqrt{B}+|T_r(\omega 2)|^2\sqrt{EB+G+J_{gr}^2J_{gn}^2B^2}\sqrt{B}}}{\sqrt[4]{B^2I^2+B^3(J_r\sqrt{E}+c_LJ_{gr}J_{gn})^2+k_L^2k_H^2(J_r+J_{gr}+J_{gn})^2+D^2(J_r+J_{gr}+J_{gn})^2B+J_r^2J_{gr}^2J_{gn}^2B^4}}, \tag{9b}$$

where T_r and T_g are the rotor and generator torques, respectively.

The frequency domain angular velocity error function of a theoretically undamped system under excitation at natural frequencies is unbounded. Therefore, performing a sensitivity analysis to find the relation between the variations of the amplitude of response at natural frequencies and the variations of system parameters which can represent the system faults is not possible. However, a physical system in practice has damping. The response of a damped system at natural frequencies is bounded due to the influence of damping in the system. Therefore, monitoring the variations of the amplitude of response in the natural frequencies can be related to variations of the system parameters and faults. In the continued part, the possibility of using the amplitude of response of a damped system at natural frequencies for monitoring the variations in the system is discussed. The results of this study can also be used for estimation of damping in the system.

As it can be seen from eq. (9), in difference with the equations for the system natural frequencies and mode shapes, the amplitude of response at the first and second natural frequencies is proportional to not only the system parameters but also the loads. The latter limits the application of amplitude of response as a fault precursor. However, it can be used as a criterion to evaluate the results obtained by the proposed fault detection algorithm, so that it provides inputs for drivetrain CM based on monitoring the variations of amplitude of response at the natural frequencies in terms of variations in the system parameters by sensitivity analysis which is elaborated in Section 3. The results of analysis of amplitude of response also provides necessary inputs for the estimation of damping in the system.

By using the simplified model in eq. (1), the peak frequency of the amplitude of response has the relation as described by eq. (10) with the associated undamped natural frequency. This result can be extended to the higher order systems and higher order natural frequencies. Our analytical study on the extreme points of the amplitude of response in higher order models shows that these points are highly nonlinear and complicated functions of system parameters which make the utilization of these equations computationally expensive. However, these points can be related to the undamped natural frequencies by using the damping coefficients as [29]

$$\Omega^i_{peak} = \Omega^i_n\sqrt{1-2\zeta_i^2}. \tag{10}$$

The two following equations can be used to estimate the damping coefficients of different modes at different operating speeds, by using the peak frequencies and the amplitude of response at those frequencies, as follows:

$$\frac{\Omega^{i,t_1}_{peak}}{\Omega^{i,t_2}_{peak}} = \sqrt{\frac{1-2\zeta^2_{i,t_1}}{1-2\zeta^2_{i,t_2}}}, \tag{11a}$$

$$\frac{|e^{\omega}_{tot}(\Omega^{i,t_1}_{peak})|}{|e^{\omega}_{tot}(\Omega^{i,t_2}_{peak})|} = f(T_r, T_g, c_L, c_H, k_L, k_H, J_r, J_{gr}, J_{gn}), \tag{11b}$$

where $\zeta_{i,t}$ is the damping coefficient related to the mode i and operation t. $|e^{\omega}_{tot}(\Omega_{peak})|$ is the amplitude of response at the peak frequency. Both the peak frequency and amplitude of response at peak frequency are estimated from the frequency domain response based on the theory elaborated earlier in this Section. The eq. (11b) is long and nonlinear with dependency to all the system parameters and loads so that relating the variations in the amplitude of response to variations in damping

coefficient seems to be a challenging task. The theory related to the employment of sensitivity analysis for relating the ratio of amplitude of response to the ratio of damping coefficients from eq. (11) and the implementation of this approach will be discussed in the continued Section. From the peak frequency and the approximated damping coefficient, the undamped frequency can be estimated by using eq. (10).

3. Drivetrain condition monitoring by using torsional measurements

The estimation of system modes by using the angular velocity error function was elaborated in Section 2. As discussed earlier, the estimated modes and the amplitude of response at those frequencies can be related to the system parameters and faults. In order to establish this relationship to be used in the proposed fault detection approach, sensitivity analysis is employed.

3.1. Sensitivity analysis

This part is aimed to obtain the closed form mathematical relationships between the drivetrain dynamic properties and amplitude of response with the drivetrain reduced-order model parameters through a sensitivity analysis for a subsequent use in the proposed fault diagnosis algorithm. Similar to in Section 2, the general 3-DOF damped torsional model of drivetrain is selected for the analytical studies in this Section.

As discussed earlier, faults like crack in shafts and rotor, coupling damage, or damage in gearbox are examples of potential faults which can change the drivetrain stiffness. For example, a shaft crack results in reduction of the torsional stiffness of the shaft [30]. A change in the stiffness influences the drivetrain system frequency modes. Therefore, by obtaining the mathematical relationship between the stiffness of different shafts and the system modes, it is possible to monitor their conditions by monitoring the variations in the system natural frequencies and normal modes. The other parameter which can influence the drivetrain torsional modes is the moment of inertia of the drivetrain components. Variations in the moment of inertia matrix represents the other category of faults in the driveline with the unbalance and loss of mass as the foremost. For example, unbalance faults are characterized by the increase of moment of inertia due to an additional force that is generated during those conditions based on the parallel axis theorem. The mathematical relationship between the drivetrain torsional natural frequencies and the moment of inertia of components can help to identify these faults. The variations in stiffness and inertia can result in similar natural frequency variation patterns. Therefore, to distinguish between variations in the natural frequencies because of variations in the shafts' stiffness with those due to variations in moment of inertia matrix (source of fault), determining the correlation between the system parameters and the normalized mode shapes can provide a useful direction to find the source of fault. The correlation between the amplitude of response at the system natural frequencies can also be useful in two ways: first, to estimate the damping coefficients and subsequently the undamped natural frequencies from the estimated natural frequencies; second, to confirm or repeal the results obtained about the system faults taken based on the analysis of natural frequencies and normal modes.

In order to achieve the above described purposes, two different sets of sensitivity analyses are performed in this Section. First, a sensitivity analysis on torsional frequencies and normal modes of the equivalent undamped system to extract drivetrain system-level CM features. Second, a sensitivity analysis on the amplitude of response at the natural frequencies primarily to estimate the damping coefficient and subsequently the undamped natural frequencies which are required for the first analysis, and then to support the CM features obtained in the first sensitivity analysis.

In order to check how the variations in stiffness and moment of inertia influence the system torsional natural frequencies and mode shapes, a sensitivity analysis is performed. There are two classes of sensitivity analysis methods, namely local and global sensitivity analysis. Morio *et al.*[31] has reported the same kind of results by using these two method for simple models. Local sensitivity determines how a small perturbation near an input parameter value influences the value of the output. In this Section, in order to find the parameters with the greatest impact on the drivetrain dynamic characteristics, local sensitivity analysis is employed due to two main reasons. First, the motivation of this work is detecting faults in early stages for predictive maintenance purposes so that variations in the drivetrain system parameters happen with a slight change around the set point values. Second, local sensitivity analysis derives a closed form expression for the sensitivity value which makes the result more reliable and easier to implement. Local sensitivity is defined as the partial derivative of the output function with respect to the input parameters [33] as

$$\boldsymbol{S}_{k,l}^{Loc} = \frac{\delta \boldsymbol{y}_k}{\delta \boldsymbol{x}_l},\ \boldsymbol{y}_k \in \{\boldsymbol{y}_1, \ldots, \boldsymbol{y}_p\}\ and\ \boldsymbol{x}_l \in \{\boldsymbol{x}_1, \ldots, \boldsymbol{x}_q\}, \tag{12}$$

where $\boldsymbol{y}_k$ is the k^{th} output and $\boldsymbol{x}_l$ is the l^{th} input. To neutralize the impact of large/small inputs and small/large outputs, the local sensitivity can be normalized by the nominal values of inputs and outputs by

$$\boldsymbol{S}_{k,l}^{Norm} = \frac{\boldsymbol{x}_l^{ref}}{\boldsymbol{y}_k^{ref}} \frac{\delta \boldsymbol{y}_k}{\delta \boldsymbol{x}_l}, \tag{13}$$

with $\boldsymbol{x}_l^{ref}$ and $\boldsymbol{y}_k^{ref}$ as the nominal values of $\boldsymbol{x}_l$ and $\boldsymbol{y}_k$. For the 3-DOF torsional model described in Section 2.1, the input and output vectors for sensitivity analysis are

$$\boldsymbol{x} = \{k_L,\ k_H,\ J_r,\ J_{gr},\ J_{gn},\ c_L,\ c_H,\ T_r,\ T_g\}, \tag{14a}$$

$$\boldsymbol{y} = \{\Omega_1^{tor},\ \Omega_2^{tor},\ \Psi_{rot}^{\Omega_1},\ \Psi_{rot}^{\Omega_2},\ \Psi_{gear}^{\Omega_1},\ \Psi_{gear}^{\Omega_2},\ \Psi_{gen}^{\Omega_1},\ \Psi_{gen}^{\Omega_2},\ |e_{tot}^{\omega}(\Omega_1^{tor})|,\ |e_{tot}^{\omega}(\Omega_2^{tor})|\}. \tag{14b}$$

where $|e_{tot}^{\omega}(\Omega_1^{tor})|$ and $|e_{tot}^{\omega}(\Omega_2^{tor})|$ are the amplitude of response at the first and second natural frequencies, respectively. The closed form of equations after applying normalized local sensitivity theory on eqs. (A.1) and (A.2) are shown in B.1 and B.2. A positive value in this analysis stands for a direct relationship between the input parameter and output, whereas a negative value represents that the parameter and output are inversely correlated. The normalized local sensitivity analysis can take different values. If the absolute value is equal to 1, it means that the relative variation in input parameter is equally transmitted to the output, whereas the absolute value higher than 1 shows that the relative variation is magnified in the output. However, the absolute value lower than 1 represents that the relative variations of the input is shrunk in the output.

In the second study, in order to find the parameters/variables which have the highest contribution in variations of the amplitude of response at the response peak frequencies, a local sensitivity analysis is performed. For this purpose, two methods are proposed. First, the peak frequencies are approximated with the associated natural frequency and subsequently the eq. (9) is used. The closed form equations which specify the correlation between the angular velocity error function amplitude at the natural frequencies with the system parameters and loads are derived by performing local sensitivity analysis as shown in B.3. This approximation can be improved by using the approximated damping coefficients and updating the eq. (9) by using the eq. 10. Another approach which is based on numerical calculations and is also used later in the simulation studies for comparison purposes is to numerically find the peak frequencies of the response in the eq. (A.5) and finding the sensitivity of the response equations to the parameters after replacing the numerically calculated frequencies in the response function. The precision in estimation of the damping coefficient by the two proposed methods compared to the approximation proposed in [23] is presented in simulation studies. In order to attain the accuracy of these methods, the results are compared to the exact values of the coefficients based on the model parameters.

The following procedure summarizes the modal estimation approach:

1. The torsional response error function (or interchangeably the low-pass filtered signal of a single torsional response) is generated. The response can be angular velocity/acceleration.
2. The resultant signal is preprocessed so that the defect frequencies of the components and structural motions-induced harmonics are filtered. The result will give the damped torsional natural frequencies of the drivetrain system.
3. The measured natural frequency is validated by the analysis of variations of amplitude of response in the suspicious frequencies at different operating speeds. In simple words, the variation of the amplitude of response in the system natural frequency (damped natural frequencies) due to the variation of damping coefficient is more significant compared to the variation of the amplitude of response in the harmonics. The variation of damping coefficient is due to the frequent variations in the operating speed in wind turbine drivetrains.
4. Damping at the natural frequency depends on the operating speed. The damping coefficient at two ensuing operations in two different speeds can be estimated by applying the theory developed in this Section and modeled by eq. 11, based on monitoring the variations of the natural frequency and amplitude of response between two sequential operations.
5. By using the estimated damped natural frequencies from torsional response and the estimated damping coefficient from the analysis of amplitude of response, the undamped natural frequencies are obtained, which provide inputs for the drivetrain system health monitoring approach based on monitoring the variations of system dynamic properties.

The algorithm which summarizes the proposed drivetrain modal estimation and the ensuing CM approach is illustrated by the flowchart in Fig. 1. $\boldsymbol{\Psi}_m^{\Omega 1}$ and $\boldsymbol{\Psi}_m^{\Omega 2}$ are the normal modes related to the 1*st* and 2*nd* natural frequencies, respectively. m varies from 1 up to the degree of the model, which accounts for the different bodies in the equivalent reduced order model. $\boldsymbol{\tau}_{\Omega}^{tor}$ and $\boldsymbol{\tau}_{\Psi_m}$ are the low-limit threshold natural frequency and normal mode related to normal operations. Close modes are more difficult to identify than well-separated modes and their identification often has an uncertainty. For wind turbine drivetrain, lower natural frequencies are in general well separated and close modes might happen only for higher modes [34].

4. Simulation studies

4.1. Simulation test case

For the simulation studies, DTU 10 MW reference wind turbine is selected. In order to evaluate if the input torque is able to excite the drivetrain natural frequencies and subsequently to study the possibility of observing those frequencies in the different drivetrain torsional responses, an effective approach is involving decoupled simulation technique. For this purpose, the rotor torque T_r of a detailed model of 10 MW turbine with a spar floating platform obtained from SIMA global simulation software [35] is used, and the impacts on the drivetrain is studied by using a decoupled analysis. The generator torque T_r is also decided to set the speed on the shaft under variable input torque, but the internal dynamics of the generator in tracking the defined set point is neglected.

The decoupled simulation approach consists of two separated phases. In the first phase, global simulation analyses are performed under different environmental conditions. In the global simulation, the blades and hub assembly, the structural module including the flexible multi-body systems for tower and platform and the nacelle are modelled. This model is coping

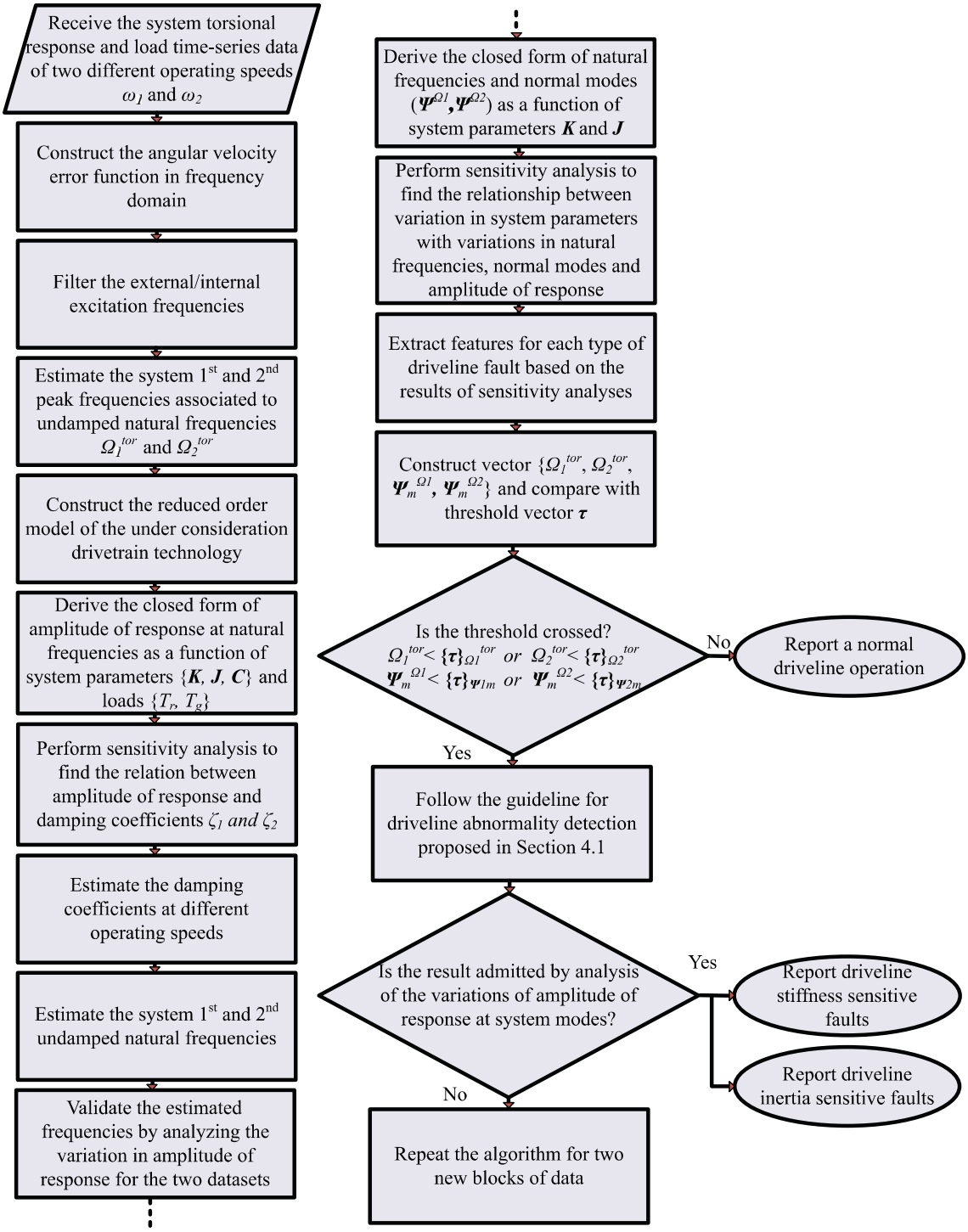

Fig. 1. Proposed algorithm for driveline condition monitoring by using torsional measurements and estimated modes.

with combined aerodynamic and hydrodynamic loading by using numerical and probabilistic models of wind, waves and current in the global simulation software to capture the integrated effect of the loads and the wind turbine control system on the turbine model. The results of the global analysis in this study are the loads transmitted to the drivetrain by the rotor specified by the time series of the resultant moment on the rotor. The second phase of decoupled analysis is that the offline global simulation results will then be applied as inputs on the drivetrain model in Simpack multi-body simulation

Table 1
10 MW medium-speed drivetrain 3-DOF model specification.

Parameter	Value
Equivalent rotor moment of inertia J_r $(kg.m^2)$	800,000,000
Equivalent gearbox moment of inertia J_{gr} $(kg.m^2)$	1,239,300
Equivalent generator moment of inertia J_{gn} $(kg.m^2)$	15,716,775
Equivalent low-speed shaft torsional stiffness k_L $(N.m/rad)$	$2,452,936,425$
Equivalent high-speed shaft torsional stiffness k_H $(N.m/rad)$	$245,293,642,500$

Table 2
Sensitivity of natural frequencies and normal modes to variations of model parameter (stiffness and inertia).

Sensitivity / Variable	k_L	k_H	J_r	J_{gr}	J_{gn}
Ω_1^{tor}	**0.50**	0.00	−0.01	**−0.03**	**−0.45**
Ω_2^{tor}	0.00	**0.50**	0.00	**-0.45**	**−0.04**
ϕ_1^{rot}	0.00	0.00	**−1.00**	**0.07**	**0.93**
ϕ_1^{gear}	0.00	0.00	0.00	0.00	0.00
ϕ_1^{gen}	0.00	0.00	0.00	0.00	0.00
ϕ_2^{rot}	**0.99**	**−0.99**	**−1.00**	**0.89**	**0.08**
ϕ_2^{gear}	0.00	0.00	0.00	−0.01	0.01
ϕ_2^{gen}	−0.01	0.01	0.00	**0.96**	**−1.00**

(MBS) software [36] to calculate and analyse the drivetrain components local dynamic responses for modal estimation and fault detection purposes. The drivetrain model in the second phase of decoupled simulation utilizes the components reduced order models. As a complementary step, the post processing of local responses provides useful information for the drivetrain secondary studies. Without loss of generality, a geared drivetrain technology is selected for the simulation studies. However, the 3-DOF reference model can also be used for direct-drive technology fault detection based on the proposed approach, where regarding the considerable mass of main shaft, it should be modelled as a separate mass to improve the model accuracy, and then a similar approach can be engaged.

The operating condition for the global simulation is close to the rated operation with an average wind speed U_w=11 m/s, significant wave height H_s=3.5 m and peak period T_p=7.5 s. In the under consideration 3-DOF torsional model of the geared drivetrain, rotor, gearbox and generator are modelled with equivalent moment of inertia, and the low- and high-speed shafts are each modelled with constant torsional stiffnesses. The generator and gearbox specifications are used from the optimized 10 MW medium-speed drivetrain system proposed in [32]. The parameters of this model are listed in the Table 1. The undamped natural frequencies of this model calculated by eq. (A.1), and validated by Simpack are 1.9 Hz and 73.9 Hz. The actual damping of the low- and high-speed shafts are also assumed to be 5% and 10% of the low-speed shaft stiffness, respectively. The torsional responses of rotor and generator shafts are obtained from the MBS model to investigate possibility of observing the natural frequencies from the angular velocity, acceleration and displacement error functions. The proposed methods for estimation of damping coefficients in different operating speeds are tested on the damped model of under consideration 10 MW geared drivetrain. The possibility of detecting different stages of system-level inertia and stiffness related faults from the torsional response obtained from the 10 MW MBS model are investigated by using the proposed algorithm.

In order to capture the system dynamic properties in the proposed approach and to get statistically comparable results, the time interval of each block of data should be large enough to capture the lowest natural frequency. The sampling frequency should be high enough to capture the higher frequency modes which are of significance, and on the other side is limited to the SCADA sampling frequency in case of implementation in the farm level. Since the realization of the method is based on the 1*st* and 2*nd* nonrigid modes, for observing these two modes, the required length of data block is only a fraction of one second and the required sampling frequency is around 400 Hz for 10 MW medium-speed drivetrain technology.

4.2. Sensitivity analysis results

The results of the normalized local sensitivity analyses with natural frequencies $(\Omega_1^{tor}, \Omega_2^{tor})$ and normal modes (ϕ_1, ϕ_2) as the outputs and shaft stiffnesses (k_L, k_H) as the inputs with variation of only one model parameter at a time are shown in the Table 2. The interpretation of the local sensitivity analysis values is disclosed in Section 3.1. The reported numbers show the normalized sensitivity values which are calculated based on 10 MW drivetrain model parameters. The values of the table in bold designate the absolute sensitivity values higher than 0.01, which is used as the criterion that the associated parameter and output are correlated. The values which are not highlighted designate the absolute sensitivity values lower than 0.01 representing a negligible sensitivity, so that the associated parameter and output are uncorrelated. As it can be seen, there is a direct relationship between the 1*st* frequency and k_L, and the 2*nd* frequency and k_H. Therefore, variations in the natural frequencies can be translated into the variations in the shaft stiffness and subsequently the defects in the drivetrain shafts. The influence of the shafts defect (stiffness variation) on the normal mode of the 1*st* natural frequency is

Table 3
Sensitivity of amplitude of response at 1*st* and 2*nd* modes to system parameters and loads.

Variable / **Sensitivity**	Method 1 (1*st* mode)	Method 2 (1*st* mode)	Method 1 (2*nd* mode)
J_r	**0.02**	**0.02**	0.01
J_{gr}	**−0.02**	−0.01	**0.21**
J_{gn}	**−0.21**	**−0.10**	**−0.47**
k_L	**−0.21**	**−0.34**	0.00
k_H	0.00	0.00	**−0.25**
c_L	**−0.08**	**−0.07**	0.00
c_H	0.00	0.00	−0.01
T_r	−0.01	−0.01	−0.01
T_g	**0.51**	**0.51**	**0.51**

negligible. However, the stiffness variation results in variations in the normal mode element of the 2*nd* natural frequency related to rotor. The results of the sensitivity analyses with natural frequencies and normal modes as the outputs and moment of inertia (J_r, J_{gr}, J_{gn}) as the inputs (variation of only one model parameter at a time) are shown in the Table 2. As it can be seen, there is an inverse relationship between the 1*st* frequency and J_{gn}, and the 2*nd* frequency and J_{gr}, so that the reduction of natural frequencies can be due to a rise in the moment of inertia. To distinguish between the drop in natural frequencies due to variation in stiffness and moment of inertia, the results should be interpreted together with monitoring the variations of normal modes. The simultaneous drop of the 1*st* frequency and the normal mode element of the 2*nd* frequency related to rotor represents an abnormality in low-speed shaft. The drop of the 2*nd* frequency and the simultaneous rise in the normal mode element of the 2*nd* frequency related to rotor discloses the problems in high-speed shaft. The drop of the 1*st* frequency, the simultaneous rise in the normal mode element of the 1*st* frequency related to rotor and drop in the normal mode element of the 2*nd* frequency related to generator reveal unbalances in generator side. The drop of the 2*nd* frequency and a simultaneous rise in the normal mode elements of the 2*nd* frequency related to both generator and rotor can be used as the criteria to detect an unbalance in gearbox.

As discussed earlier in Section 3, another criterion which can be used in parallel to ascertain the validity of the above guideline is monitoring the variations of the amplitude of response at the natural frequencies based on the sensitivity analysis values reported in the Table 3 which will be discussed later in this Section. This criterion in difference with the criteria established in the above guideline needs an anterior estimation of the system loads. However, a good estimation of both the rotor and generator torques is available in wind turbine application. The rotor torque is estimated by using the blade aerodynamic equations and the input wind. The generator torque is estimated from the generator voltage and current measurements.

Sensitivity of the amplitude of frequency spectrum of angular velocity error function at the 1*st* mode to system parameters and loads are summarized in the Table 3. The 2*nd* column is related to the first method based on the approximation of peak frequencies with the associated natural frequencies, calculating the response equation at those frequencies, deriving the sensitivity equations of the resulted functions in terms of parameters, then updating the response based on the approximated damping coefficients and repeating the sequence to improve the accuracy of estimation. The results reported of the first method are obtained by only a single iteration. The use of this method based on the approximation of Ω_{peak} with Ω_n which is more accurate if $\zeta << 1$. However, the accuracy can be improved as explained by the correction which can be applied on the eq. (9) based on the estimated damping coefficients. The 3*rd* column of this table is related to the second method based on the numerical calculation of peak frequencies, deriving the response equation in those frequencies and finding the sensitivity of the resulted equations to the parameters and loads variations. The sensitivity of the amplitude of frequency spectrum of angular velocity error function at the 2*nd* mode to system parameters and loads are also listed in the 4*th* column of the same table.

As it can be seen from the Table 3, variation in amplitude of response at the 1*st* mode is mainly dominated by generator torque, generator inertia, low-speed shaft stiffness and damping. The amplitude ratio at the 1*st* mode for two different operations is directly influenced by load and inversely influenced by damping. Knowing that the system parameters are constant, by a prior knowledge about the load, variations in damping can be estimated. To estimate the damping coefficients from the amplitude of response based on the sensitivity analysis results, three different cases can be assumed for the simulations. All these cases are based on monitoring the variations of the response amplitude at the natural frequencies between two different operating points t_1 and t_2.

Case 1: The two operating points are close, so that the system parameters and load stay constant.

In this case, the variation in the amplitude ratio directly reflects the variation in the actual damping ratio which varies due to the variation of the operating speed. Those variations are correlated proportional with the numbers calculated by the sensitivity analysis. From this relationship, the variation in the damping coefficient is estimated. By using this information along with eq. (11a), the two dampings of the two operations are estimated. It is worth noting that in Case 1, since the system parameters and subsequently the critical dampings are constant, the actual damping ratio is equal to the ratio of the damping coefficients between the two operations. The estimated values of damping coefficients at the 1*st* mode in two different operating speeds which meet the conditions of Case 1, by using the two proposed methods which described in Section 3.1 compared to the approximation proposed in [23] are listed in the Table 4. The comparison of the three methods

Table 4
Estimation of damping coefficient at the 1*st* mode for Case 1: loads do not change between the two operating points.

Operation	ω ($\frac{rad}{s}$)	Ω^1_{peak} ($\frac{rad}{s}$)	$\lvert e^{\omega}_{tot}(\Omega^1_{peak})\rvert$	ζ (reference model)	ζ (method 1)	ζ (method 2)	ζ (method in [23])
ω_1	0.9	8.67	0.159	0.21	0.20	0.16	0.48
ω_2	0.7	8.46	0.156	0.26	0.25	0.22	0.49

Table 5
Estimation of damping coefficient at the 1*st* mode for Case 2: loads change between the two operating points.

Operation	ω ($\frac{rad}{s}$)	Ω^1_{peak} ($\frac{rad}{s}$)	$\lvert e^{\omega}_{tot}(\Omega^1_{peak})\rvert$	ζ (reference model)	ζ (method 1)	ζ (method 2)	ζ (method in [23])
ω_1	0.9	8.67	0.159	0.21	0.21	0.18	0.27
ω_2	0.7	8.46	0.171	0.26	0.25	0.23	0.31

of estimating damping coefficients shows that the method 1 even based on one iteration outperforms the two other damping approximation approaches by demonstrating a much lower relative error.

Case 2: The load varies between the two operations but the system parameters stay constant.

In this case, the loads and dampings vary while the other system parameters are constrained to be constant. With an access to the estimated load it is still possible similar to in Case 1 to measure the variation in damping coefficients by using the local sensitivity analysis results and by relating the variation in response amplitude to the variation in load and damping, based on the proportions calculated by the sensitivity analysis. From this relationship, the variation in the damping coefficient and subsequently the two dampings of the two operations are estimated similar to in Case 1. The estimated values of damping coefficients at the 1*st* mode in two different operating speeds which meet the conditions of Case 2, by using the two methods proposed in Section 3.1 are listed in the Table 5. It is assumed that during the second operating speed/condition, both the rotor and generator loads have been increased by 20% so that $\frac{T_r^{\omega_2}}{T_r^{\omega_1}} = \frac{T_g^{\omega_2}}{T_g^{\omega_1}} = 1.2$. Similar to in Case 1, the comparison of the three methods of estimating damping coefficients shows that the method 1 even with one iteration outperforms the two other damping approximation approaches.

Case 3: Both the load and parameters are changing.

In this case, the estimation of damping variation from the response is challenging because it needs a good estimation not only from the load but also the other system parameters. In this case, the amplitude of response may not give enough information to estimate the damping coefficients based on that, because the updated values for the system parameters may be unknown. However, assuming that the load can be estimated, the result of this study can be used to authenticate the conclusions made about the system faults from the analysis of natural frequencies and normal modes variations.

A similar set of sensitivity analysis is performed for the second mode which shows the sensitivity of amplitude of response at the second natural frequency more significantly to the high-speed shaft stiffness, generator torque, and the moment of inertia of gearbox and generator with no considerable sensitivity to the damping at the second mode. Based on this study,the amplitude of response at the second frequency is not significantly influenced by the value of the dampings so that the amplitude of response is not recommended as a good criterion for estimation of damping coefficient of the second mode. Some other functions of the amplitude of response of different operations may offer less sensitivity to parameters variation which are more useful when the information on the system is low, which are not discussed in here. Another potential of monitoring the variations of amplitude of response at the estimated torsional natural frequencies is for estimation of the loads. In other words, for the same operational speed and system parameters, the natural frequencies and dampings will stay the same and variations of the amplitude of response at system torsional natural frequencies is directly connected to variations in generator torque which can be used for monitoring the variations of the torque. The latter is also not discussed more in this work.

The extracted features obtained by the sensitivity study for detecting the drivetrain faults are evaluated by both the MBS simulation model and the real operational data in the continued parts.

4.3. Simulation-based validation of proposed modal estimation and condition monitoring approach

The simulation-based validations relies on the data obtained from the multi-body simulation model of 10 MW medium-speed PMSG drivetrain system in Simpack.

4.3.1. Estimation of natural frequencies from torsional measurements

The PSD spectrum of angular velocity error function obtained from 10 MW drivetrain model and its capability in highlighting the torsional natural frequencies is shown in Figs. 2 (b)-2(d). In these three figures, the performance of angular velocity error function in extracting the 1*st* and 2*nd* torsional natural frequencies of the drivetrain is compared with angular displacement and angular acceleration error functions. As it can be seen, acceleration error function outperforms in revealing the higher frequency modes (the 2*nd* mode). The higher modes have usually a lower impact on the response, which impedes disclosure of those frequencies. The PSD spectrum of the input torque applied on the drivetrain MBS model

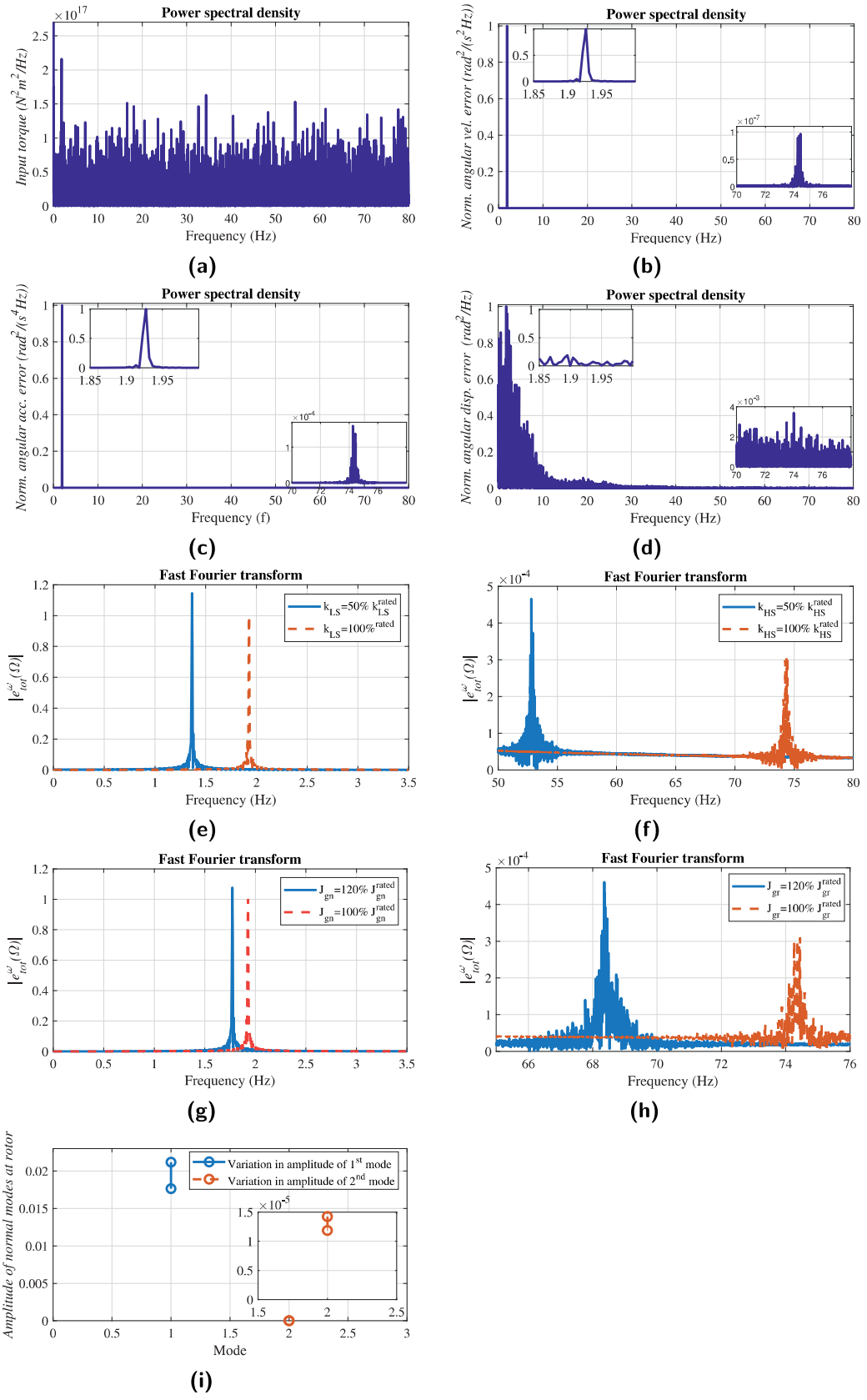

Fig. 2. Simulation results based on 10 MW floating wind turbine model. (a) PSD of τ^{rotor}. (b) PSD of e^{vel}_{tot}. (c) PSD of e^{acc}_{tot}. (d) PSD of e^{dis}_{tot}. (e) Fault in low-speed shaft. (f) Fault in high-speed shaft. (g) Fault in generator. (h) Fault in gearbox. (i) Fault in rotor.

Table 6
Low-speed shaft fault cases.

Fault case	$\frac{k_L}{k_L^n}$	$\frac{\Omega_1^{tor}}{\Omega_1^{tor.n}}$	$\frac{\Omega_2^{tor}}{\Omega_2^{tor.n}}$	$\frac{\Psi_{rot}^{\Omega_1}}{\Psi_{rot}^{\Omega_1.n}}$	$\frac{\Psi_{rot}^{\Omega_2}}{\Psi_{rot}^{\Omega_2.n}}$	$\frac{\Psi_{gear}^{\Omega_1}}{\Psi_{gear}^{\Omega_1.n}}$	$\frac{\Psi_{gear}^{\Omega_2}}{\Psi_{gear}^{\Omega_2.n}}$	$\frac{\Psi_{gen}^{\Omega_1}}{\Psi_{gen}^{\Omega_1.n}}$	$\frac{\Psi_{gen}^{\Omega_2}}{\Psi_{gen}^{\Omega_2.n}}$
*LC*0	1	1	1	1	1	1	1	1	1
*LC*1	0.95	0.975	1.000	1.000	0.950	1.000	1.000	1.000	1.000
*LC*2	0.85	0.923	0.999	1.000	0.851	1.001	1.000	1.000	1.001
*LC*3	0.7	0.838	0.999	1.000	0.000	1.003	1.000	1.000	1.003
*LC*4	0.5	0.709	0.998	1.000	0.000	1.005	1.000	1.000	1.005

Table 7
High-speed shaft fault cases.

Fault case	$\frac{k_H}{k_H^n}$	$\frac{\Omega_1^{tor}}{\Omega_1^{tor.n}}$	$\frac{\Omega_2^{tor}}{\Omega_2^{tor.n}}$	$\frac{\Psi_{rot}^{\Omega_1}}{\Psi_{rot}^{\Omega_1.n}}$	$\frac{\Psi_{rot}^{\Omega_2}}{\Psi_{rot}^{\Omega_2.n}}$	$\frac{\Psi_{gear}^{\Omega_1}}{\Psi_{gear}^{\Omega_1.n}}$	$\frac{\Psi_{gear}^{\Omega_2}}{\Psi_{gear}^{\Omega_2.n}}$	$\frac{\Psi_{gen}^{\Omega_1}}{\Psi_{gen}^{\Omega_1.n}}$	$\frac{\Psi_{gen}^{\Omega_2}}{\Psi_{gen}^{\Omega_2.n}}$
*LC*0	1	1	1	1	1	1	1	1	1
*LC*1	0.95	1.000	0.975	1.000	1.052	1.000	1.000	1.000	1.000
*LC*2	0.85	0.999	0.923	1.000	1.175	0.998	1.000	1.000	0.998
*LC*3	0.7	0.998	0.838	1.000	1.423	0.996	1.000	1.000	0.996
*LC*4	0.5	0.996	0.710	0.993	1.983	0.991	1.000	1.000	0.991

is shown in Fig. 2(a). This torque which is obtained from the global simulation contains the majority of frequency components and can excite the drivetrain natural frequencies.

4.3.2. Diagnosis of drivetrain faults

The drivetrain faults at system-level vary the equivalent torsional model parameters, so that by monitoring the consequences of these variations on the drivetrain dynamic properties and amplitude of response at the natural frequencies these faults can be detected. For simulation purposes, the faults are simulated independently so that the correlations between the under consideration faults are neglected.

As discussed earlier, detection of stiffness changing related faults is possible in the proposed approach by monitoring the consequences of these faults on the drivetrain torsional modes based on the results of sensitivity analysis. As an example of stiffness-related faults, the growth of crack in the shaft causes the torsional stiffness of the shaft to decrease and this change will be reflected in the driveline torsional natural frequencies. The variations of the shafts stiffness from 5% are considered as the start of fatigue crack in the shaft. The latter is equivalent with variation in the modal parameters as the fault precursors in the proposed CM algorithm. In order to simulate the shaft crack growth in the low- and high-speed shafts, the torsional stiffness of these two shafts in the Simpack model is reduced in four steps from 5 to 50%. The subsequent changes in the undamped natural frequencies and normal modes are listed and shown in the Tables 6 and 7. As it can be seen from these tables, the simulation results agree with the results obtained from the analytical sensitivity analysis of natural frequencies and normal modes reported in the Table 2. Since the fault detection features are obtained from the variations of the physical model, the threshold for these features is accordingly specified based on the sensitivity analysis employed on a specific drivetrain.

The reduction of the 1*st* natural frequency due to a crack in low-speed shaft is illustrated in Fig. 2(e). In addition, as it can be seen from this figure, for the two operations with the same loading conditions, that one of them is the normal system and the other one is the system with a crack in the low-speed shaft, the amplitude of response at the 1*st* natural frequency is higher in the system with the cracked shaft compared to the normal system, which agrees with the results of the analytical sensitivity analysis of the amplitude of response as reported in the Table 3. The influence of crack in high-speed shaft and the consequence in drop of the 2*nd* natural frequency is shown in Fig. 2(f). As it can also be seen in this figure, a crack in the high-speed shaft causes an increase in the amplitude of response at the 2*nd* natural frequency, which agrees with the sensitivity results related to the amplitude of response at the 2*nd* mode as mentioned in the Table 3. For scaling and demonstration purposes, Figs. 2(e) and 2(f) are normalized with the normal system results.

The detection of inertia changing related faults is also possible by monitoring the consequences of these faults on the drivetrain torsional modes based on the performed sensitivity analysis results. As an example of inertia-related faults, unbalance in the rotor, gearbox or generator shafts results in an increase in the equivalent inertia of the component in the model. Dependent on the severity of unbalance the variation in inertia will be different. A slight unbalance can cause a very slight change in the inertia and subsequently a slight change in the modes which makes the detection challenging by the proposed approach. In here, in order to simulate the severe unbalance faults, the inertia of the associated component is increased in three steps from 5 to 20%. The subsequent changes in the drivetrain modes are listed and shown in the Tables 8-10. The simulation results agree with the sensitivity analysis results presented in the Table 2.

The reduction of 1*st* and 2*nd* natural frequency due to increase of inertia of generator and gearbox as a result of unbalance faults in generator and gearbox are respectively shown in Figs. 2(g) and 2(h). The influence of increase of rotor inertia, which can model the rotor unbalance fault, on the simultaneous reduction of 1*st* and 2*nd* normal modes in rotor position is also shown in Fig. 2(i). All these three figures are normalized with the normal system results.

Table 8
Inertia related fault cases (rotor).

Fault case	$\frac{J_r}{J_r^H}$	$\frac{\Omega_1^{tor}}{\Omega_1^{tor.n}}$	$\frac{\Omega_2^{tor}}{\Omega_2^{tor.n}}$	$\frac{\Psi_{rot}^{\Omega_1}}{\Psi_{rot}^{\Omega_1.n}}$	$\frac{\Psi_{rot}^{\Omega_2}}{\Psi_{rot}^{\Omega_2.n}}$	$\frac{\Psi_{gear}^{\Omega_1}}{\Psi_{gear}^{\Omega_1.n}}$	$\frac{\Psi_{gear}^{\Omega_2}}{\Psi_{gear}^{\Omega_2.n}}$	$\frac{\Psi_{gen}^{\Omega_1}}{\Psi_{gen}^{\Omega_1.n}}$	$\frac{\Psi_{gen}^{\Omega_2}}{\Psi_{gen}^{\Omega_2.n}}$
*LC*0	1	1	1	1	1	1	1	1	1
*LC*1	1.05	1.000	1.000	0.952	0.952	1.000	1.000	1.000	1.000
*LC*2	1.10	0.999	1.000	0.909	0.909	1.000	1.000	1.000	1.000
*LC*3	1.20	0.998	1.000	0.833	0.833	1.000	1.000	1.000	1.000

Table 9
Inertia related fault cases (gearbox).

Fault case	$\frac{J_{gr}}{J_{gr}^H}$	$\frac{\Omega_1^{tor}}{\Omega_1^{tor.n}}$	$\frac{\Omega_2^{tor}}{\Omega_2^{tor.n}}$	$\frac{\Psi_{rot}^{\Omega_1}}{\Psi_{rot}^{\Omega_1.n}}$	$\frac{\Psi_{rot}^{\Omega_2}}{\Psi_{rot}^{\Omega_2.n}}$	$\frac{\Psi_{gear}^{\Omega_1}}{\Psi_{gear}^{\Omega_1.n}}$	$\frac{\Psi_{gear}^{\Omega_2}}{\Psi_{gear}^{\Omega_2.n}}$	$\frac{\Psi_{gen}^{\Omega_1}}{\Psi_{gen}^{\Omega_1.n}}$	$\frac{\Psi_{gen}^{\Omega_2}}{\Psi_{gen}^{\Omega_2.n}}$
*LC*0	1	1	1	1	1	1	1	1	1
*LC*1	1.05	0.998	0.978	1.004	1.046	1.000	1.000	1.000	1.050
*LC*2	1.10	0.997	0.957	1.007	1.092	1.000	1.000	1.000	1.100
*LC*3	1.20	0.993	0.919	1.015	1.183	1.000	1.000	1.000	1.200

Table 10
Inertia related fault cases (generator).

Fault case	$\frac{J_{gn}}{J_{gn}^H}$	$\frac{\Omega_1^{tor}}{\Omega_1^{tor.n}}$	$\frac{\Omega_2^{tor}}{\Omega_2^{tor.n}}$	$\frac{\Psi_{rot}^{\Omega_1}}{\Psi_{rot}^{\Omega_1.n}}$	$\frac{\Psi_{rot}^{\Omega_2}}{\Psi_{rot}^{\Omega_2.n}}$	$\frac{\Psi_{gear}^{\Omega_1}}{\Psi_{gear}^{\Omega_1.n}}$	$\frac{\Psi_{gear}^{\Omega_2}}{\Psi_{gear}^{\Omega_2.n}}$	$\frac{\Psi_{gen}^{\Omega_1}}{\Psi_{gen}^{\Omega_1.n}}$	$\frac{\Psi_{gen}^{\Omega_2}}{\Psi_{gen}^{\Omega_2.n}}$
*LC*0	1	1	1	1	1	1	1	1	1
*LC*1	1.05	0.978	0.998	1.046	1.003	1.000	1.000	1.000	0.952
*LC*2	1.10	0.958	0.997	1.093	1.007	1.000	1.000	1.000	0.909
*LC*3	1.20	0.920	0.994	1.186	1.012	1.000	1.000	1.000	0.833

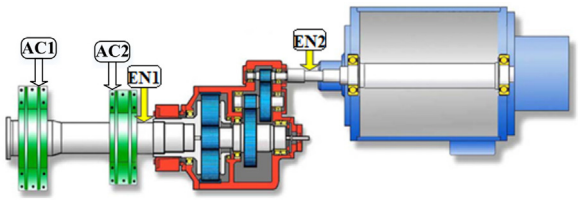

Fig. 3. Vestas V66-1.750 MW drivetrain topology, and vibration sensors placement.

5. Experimental studies

5.1. Experimental test case

The operational data from Vestas V66-1.750 MW turbine is used for the experimental study. To test the method, an additional encoder is installed on the low-speed shaft. The topology of the drivetrain is shown in Fig. 3. As it can be seen, the two encoders *EN*1 and *EN*2 are the torsional measurement sensors placed on the low- and high-speed shafts, respectively. *AC*1 and *AC*2 are the accelerometers placed on the two main bearings to measure the lateral vibrations for comparison of the proposed method based on torsional vibrations with conventional approaches in the literature which are mainly based on translational vibrations. The data sets include the drivetrain operations under different operating speeds in both normal and faulty cases.

In PSD of the angular velocity error function of the operational data, in addition to the natural frequencies, some other frequency components are also expected to be observed. However, by a prior knowledge about the defect frequencies and the other torsional excitation sources, and by subsequently filtering those frequencies, it is possible to distinguish the natural frequencies. The benefits with measuring the natural frequencies by this noninvasive method are the low implementation cost, and the possibility of obtaining the precise values of natural frequencies by including the system nonlinearities, and translational impacts on the rotation transferred through the bed-plate and torque arm.

5.2. Experimental validation of proposed modal estimation and condition monitoring approach

The experimental validations are based on the operational data obtained from the drivetrain system of a 1.75 MW Vestas wind turbine.

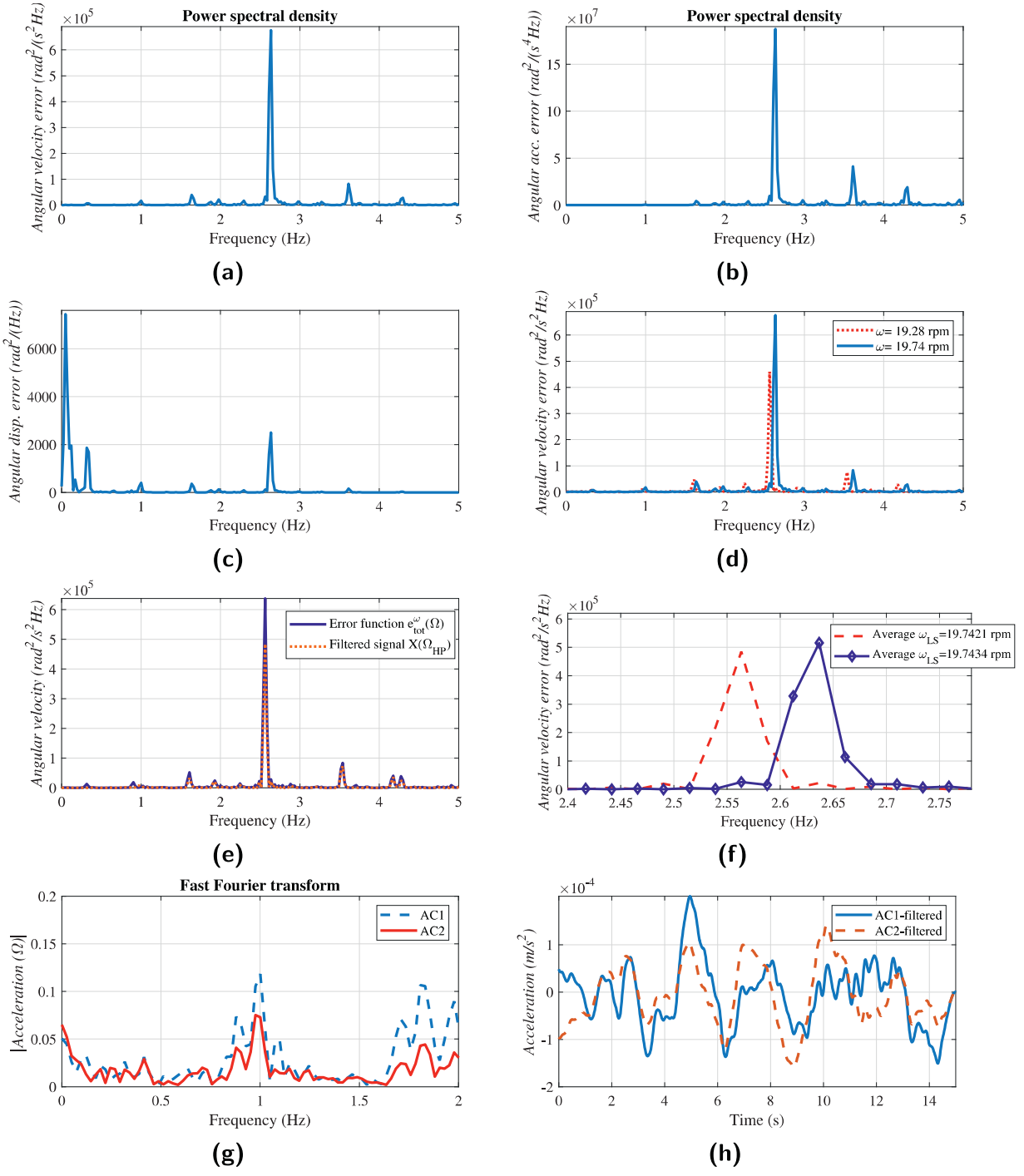

Fig. 4. Experimental results based on 1.75 MW Vestas turbine operational data. (a) PSD of e^{ω}_{tot}. (b) PSD of e^{α}_{tot}. (c) PSD of e^{θ}_{tot}. (d) PSD of e^{ω}_{tot} in two different operations. (e) Comparison of $X(\Omega_{HP})$ and $e^{\omega}_{tot}(\Omega)$ performances. (f) Fault in low-speed shaft: influence on 1*st* mode. (g) Fault in low-speed shaft: FFT of accelerometers. (h) Fault in low-speed shaft: phase difference.

5.2.1. Estimation of natural frequencies

The PSD spectrum of angular velocity error function of the Vestas drivetrain operational data for a rated operation is compared with angular displacement and acceleration error functions as shown in Figs. 4(a)-4(c), which shows the observability of both the drivetrain and blade natural frequencies. The results are validated by comparing with the 1*st* drivetrain and 1*st* blade edgewise natural frequencies of another turbine with the same drivetrain technology and a similar power range reported in [37]. The performance of angular velocity error function is compared with angular displacement and ac-

Table 11
Acceleration r.m.s compared with the warning limits brought in standard ISO 10816-21.

Comparison Sensor	*AC*1	*AC*2
Measured r.m.s ($\frac{m}{s^2}$)	0.01	0.01
Standard r.m.s threshold ($\frac{m}{s^2}$)	0.3	0.3

celeration error functions. As it can be seen, angular acceleration shows a slightly higher performance in amplification and extraction of characteristic frequencies of higher values. A comparison between the angular velocity error function PSD in two different operating speeds is shown in Fig. 4(d). As it can be seen, the higher damping coefficient in lower speeds has resulted in a lower damped natural frequency. Furthermore, at the drivetrain natural frequency, the amplitude reacts more significantly to the variation in damping. In other words, the amplitude of response at the natural frequency reduces more compared with other harmonics, for a lower rotor speed which corresponds to a higher damping. The filtered low-speed shaft angular velocity measurement is shown in Fig. 4(e). The chosen filter is a first order high-pass butterworth filter with the cutoff frequency 1 Hz. As it can be seen, the filtered signal shows some degree of competence with the angular velocity error function in extracting the torsional properties of the system *i.e.* the drivetrain and the blade in plane natural frequencies.

5.2.2. Diagnosis of the drivetrain fault

Our observation on extensive operational measurements of the drivetrain system of the under consideration turbine shows that for the same turbine rotational speed the natural frequencies do not change under normal operations. The Fig. 4(f) shows the deviation of 1*st* natural frequency which is apparently due to a low-speed shaft fatigue crack. Therefore, the method is able to detect the shaft cracks in the early stages of progression. As it can be seen, the reduction of the natural frequency at the same operational speed is observed due to a reduction in the low-speed shaft stiffness as a consequence of fault in the low-speed shaft. The frequency spectra presented in literature for detection of shaft crack are usually unreliable as other types of faults can also generate a similar frequency pattern. More advanced frequency domain approaches call for the coupled analysis of the crack vibrations consequences in all bending, longitudinal and torsion which is both expensive to implement and dependent on the load and excitation frequencies. The cracked shaft can represent a periodic reduction in the shaft stiffness due to nonlinear effects such as breathing of the crack. Dependent on the type of crack the variation of the stiffness of the different directions of lateral, axial and torsional could be different, because the stiffness change is dependent on the direction of bending moment at the crack cross-section. Due to the coupling phenomena that exists in a cracked rotor, *i.e.* bending-torsion, longitudinal-torsion, the variations of longitudinal or bending stiffness parameters, which have relationship with type and depth of crack, also influence the torsional stiffness in later stages. Therefore, the assumptions for modelling of a crack with constant torsional stiffness asymmetry does not seem to be unrealistic. However, the proposed method has a potential to be adjusted based on more complex models of stiffness variation in terms of crack properties. The performance of the proposed fault detection feature based on monitoring natural frequency variations from torsional measurements in detection of low-speed shaft faults is compared with three conventional methods in literature based on accelerometers measurements. *First*, the frequency domain indicator based on observing twice the running frequency component and the subharmonic resonance [27,38]; *second*, the variable phase difference between the time domain measurements of the accelerometers placed on the two sides of shaft at the shaft rotational frequency component; *third*, the r.m.s of time domain acceleration based on standard ISO 10816-21. The frequency spectra of the two accelerometers placed on the two main bearings which support the main shaft are shown in Fig. 4(g). In this figure, the under consideration turbine has been working with the nominal rotational speed which is 0.33 Hz in the low-speed side. As it can be seen, the main revolution frequency, the double frequency and the subharmonics do not show a significant amplitude in the response. The insufficiency of frequency domain analysis in different operating speeds in detecting shaft faults in the general rotor system is also reported in [26]. The other drawback with frequency domain analysis based on our observations is that due to the low frequency content of the low-speed shaft faults, they can be mistaken with a wide range of excitation frequencies due to environmental and structural motions induced vibrations which happen in the low frequency range. The latter is the reason that the second method which is the crack detection criterion based on the analysis of phase difference between the acceleration measurements of the two sides of low-speed shaft is also not helpful. The Fig. 4(h) shows the synchronized time domain acceleration measurements of AC1 and AC2 which are band-pass filtered around the low-speed shaft rotational frequency. As it can be seen, the figure does not represent any variation in the phase difference between these two signals. Monitoring of the variations of the phase difference of the frequency component 0.33 Hz is not guaranteed due to the influence of the other frequency components which appear in response in this frequency range. As it can be seen in the Table 11, the described abnormality cannot also be detected by the third method which is the conventional time domain approach based on the evaluation of the r.m.s value of the time series data of the translational vibrations.

It is worth noting that the experimental study is based on monitoring the variations of the natural frequency alone and not the mode shape. The result shows that the natural frequency has reduced by 3%, which in this specific case has been due to the main shaft fault. If we apply the results of analytical sensitivity analysis of drivetrain dynamic properties as the function of equivalent model parameters, which are based on 10 MW drivetrain model, to 1.75 MW model, the 3% reduction

of first natural frequency in general could happen due to either 6% reduction in the main shaft stiffness or 6% increase in the gearbox inertia. The other possibility is the combined variation of stiffness and inertia. Therefore, by using the proposed approach, for localizing the abnormality, the analysis of the mode shapes will also be required. The estimation of mode shapes from torsional response is not discussed in this paper, but it can be attained by the drivetrain equivalent model estimated by using the drivetrain torsional measurements as discussed in [34].

6. Conclusions

A condition monitoring approach bottomed on the coordination of a data-driven approach for estimation of drivetrain dynamic properties based on signal processing of the torsional measurements, and the analytical/physical model of drivetrain to extract the fault detection features was presented. It was shown that only a reduced order 3-DOF model is enough to detect different categories of drivetrain faults at system level.

The drivetrain modal estimation approach by using torsional measurements was analytically explained and then validated by using both simulation and experimental studies, so that the observability of modal frequency and the estimation of modal damping for the different modes and operating speeds were demonstrated by different investigated case studies. The estimated modes were later supporting the proposed drivetrain condition monitoring approach which works based on monitoring the variations of the system dynamic properties and amplitude of response at the drivetrain torsional frequencies. The drivetrain system fault detection features were extracted by sensitivity analysis and were tested by both 10 MW drivetrain simulated model in Simpack software and 1.75 MW Vestas operational turbine. The results were showing that the progression state of different categories of drivetrain faults at system level are observable in an early stage by the method developed based on 3-DOF equivalent torsional model of the drivetrain, only by tracking the faults consequent variations in the drivetrain dynamic properties.

The results demonstrate the potentials of torsional measurements for both drivetrain modal estimation and system-level fault detection. The future work will be devoted to the application of higher DOF torsional models as more detailed equivalent models of the drivetrain, which can capture real-time variations in mesh stiffness and inertia of individual gears and intermediate shafts, which can help to detect faults in those subcomponents by taking into account the components internal dynamics.

Declaration of Competing Interest

The authors declare that they have no known competing financial interests or personal relationships that could have appeared to influence the work reported in this paper.

CRediT authorship contribution statement

Farid K. Moghadam: Conceptualization, Formal analysis, Methodology, Validation, Visualization, Writing - original draft. **Amir R. Nejad:** Supervision, Writing - review & editing.

Acknowledgement

The authors would like to thank Kongsberg Digital AS, Trondheim, Norway, for providing experimental data for this study. The authors also would like to thank John Marius Hegseth of Norwegian University of Science and Technology, Trondheim, Norway, for providing the 10 MW spar floating wind turbine global analysis simulation data.

Appendix A. Drivetrain dynamic properties and modal analysis by using 3-DOF equivalent torsional model

A1. 3-DOF equivalent model dynamic properties as a function of model parameters

The two undamped natural frequencies (nonrigid modes) based on 3-DOF lumped-mass-spring model of a geared drivetrain, as functions of model parameters, can be calculated by

$$\Omega_1^{tor} = \sqrt{\frac{k_L}{2J_r} + \frac{k_L + k_H}{2J_{gr}} + \frac{k_H}{2J_{gn}} - \sqrt{(\frac{-k_L}{2J_r} - \frac{k_L - k_H}{2J_{gr}} + \frac{k_H}{2J_{gn}})^2 + \frac{k_L k_H}{J_{gr}^2}}}, \tag{A.1a}$$

$$\Omega_2^{tor} = \sqrt{\frac{k_L}{2J_r} + \frac{k_L + k_H}{2J_{gr}} + \frac{k_H}{2J_{gn}} + \sqrt{(\frac{-k_L}{2J_r} - \frac{k_L - k_H}{2J_{gr}} + \frac{k_H}{2J_{gn}})^2 + \frac{k_L k_H}{J_{gr}^2}}}, \tag{A.1b}$$

where Ω_1^{tor} and Ω_2^{tor} are the 1*st* and 2*nd* natural frequencies, k_L and k_H are the torsional stiffness of low- and high-speed shafts, and J_r, J_{gr} and J_{gn} are the moment of inertia of rotor, gearbox and generator, respectively.

The two normal modes related to the two non-rigid modes of the under consideration drivetrain model, as functions of model parameters, which are scaled to unity length are

$$\Psi_{rot}^{\Omega_1} = \frac{\sqrt{\frac{k_L^2}{\frac{k_H^2}{(k_H - J_{gn}A)^2} + \frac{k_L^2}{(k_L - J_rA)^2} + 1)}}}{k_L - J_rA}, \tag{A.2a}$$

$$\Psi_{rot}^{\Omega_2} = \frac{\sqrt{\frac{k_L^2}{\frac{k_H^2}{(k_H - J_{gn}B)^2} + \frac{k_L^2}{(k_L - J_rB)^2} + 1}}}{k_L - J_rB}, \tag{A.2b}$$

$$\Psi_{gear}^{\Omega_1} = \sqrt{\frac{1}{\frac{k_H^2}{(k_H - J_{gn}A)^2} + \frac{k_L^2}{(k_L - J_rA)^2} + 1}}, \tag{A.2c}$$

$$\Psi_{gear}^{\Omega_2} = \sqrt{\frac{1}{\frac{k_H^2}{(k_H - J_{gn}B)^2} + \frac{k_L^2}{(k_L - J_rB)^2} + 1}}, \tag{A.2d}$$

$$\Psi_{gen}^{\Omega_1} = \frac{\sqrt{\frac{k_H^2}{\frac{k_H^2}{(k_H - J_{gn}A)^2} + \frac{k_L^2}{(k_L - J_rA)^2} + 1}}}{k_H - J_{gn}A}, \tag{A.2e}$$

$$\Psi_{gen}^{\Omega_2} = \frac{\sqrt{\frac{k_H^2}{\frac{k_H^2}{(k_H - J_{gn}B)^2} + \frac{k_L^2}{(k_L - J_rB)^2} + 1}}}{k_H - J_{gn}B}, \tag{A.2f}$$

where

$A = -\sqrt{(\frac{k_H}{2J_{gn}} - \frac{k_L}{2J_r} + \frac{k_H - k_L}{2J_{gr}})^2 + \frac{k_H k_L}{J_{gr}^2}} + \frac{k_H}{2J_{gn}} + \frac{k_L}{2J_r} + \frac{k_H + k_L}{2J_{gr}}$, and

$B = \sqrt{(\frac{k_H}{2J_{gn}} - \frac{k_L}{2J_r} + \frac{k_H - k_L}{2J_{gr}})^2 + \frac{k_H k_L}{J_{gr}^2}} + \frac{k_H}{2J_{gn}} + \frac{k_L}{2J_r} + \frac{k_H + k_L}{2J_{gr}}$.

$\Psi_{rot}^{\Omega_1}$, $\Psi_{gear}^{\Omega_1}$ and $\Psi_{gen}^{\Omega_1}$ are normal modes at rotor, gearbox and generator due to the 1*st* mode. $\Psi_{rot}^{\Omega_2}$, $\Psi_{gear}^{\Omega_2}$ and $\Psi_{gen}^{\Omega_2}$ are the same parameters for the 2*nd* mode.

A2. Modal analysis by using the amplitude spectrum of angular velocity error function and 3-DOF equivalent model

The amplitude of angular positions at the different places of the drivetrain based on the 3-DOF equivalent torsional model of drivetrain transferred to the rotor side are as

$$|\theta_r(\Omega)| = \sqrt{\frac{\left\{(-\Omega^4 J_{gr}J_{gn} + \Omega^2(c_Lc_H + \sqrt{G}) - k_Lk_H)^2 + \Omega^2(\Omega^2\sqrt{E} - D)^2\right\}|Tr(\Omega)|^2 + \left\{(-\Omega^2 c_Lc_H + k_Lk_H)^2 + \Omega^2 D^2\right\}|T_g(\Omega)|^2}{\Omega^4\left(\Omega^4 J_rJ_{gr}J_{gn} - \Omega^2 I + k_Lk_H(J_r + J_{gr} + J_{gn})\right)^2 + \Omega^6\left(\Omega^2(J_r\sqrt{E} + c_LJ_{gr}J_{gn}) - D(J_r + J_{gr} + J_{gn})\right)^2}}, \tag{A.3a}$$

$$|\theta_{gr}(\Omega)| = \sqrt{\frac{\left\{(-\Omega^2(c_Lc_H + k_LJ_{gn}) + k_Lk_H)^2 + \Omega^2(\Omega^2 c_LJ_{gn} - D)^2\right\}|Tr(\Omega)|^2 + \left\{(\Omega^2(c_Lc_H + k_HJ_r) - k_Hk_L)^2 + \Omega^2(\Omega^2 c_HJ_r - D)^2\right\}|T_g(\Omega)|^2}{\Omega^4\left(\Omega^4 J_rJ_{gr}J_{gn} - \Omega^2 I + k_Lk_H(J_r + J_{gr} + J_{gn})\right)^2 + \Omega^6\left(\Omega^2(J_r\sqrt{E} + c_LJ_{gr}J_{gn}) - D(J_r + J_{gr} + J_{gn})\right)^2}}, \tag{A.3b}$$

$$|\theta_{gn}(\Omega)| = \sqrt{\frac{\left\{(-\Omega^2 c_Lc_H + k_Lk_H)^2 + \Omega^2 D^2\right\}|Tr(\Omega)|^2 + \left\{(-\Omega^4 J_rJ_{gr} + \Omega^2(c_Lc_H + \sqrt{H}) - k_Lk_H)^2 + \Omega^2(\Omega^2\sqrt{F} - D)^2\right\}|T_g(\Omega)|^2}{\Omega^4\left(\Omega^4 J_rJ_{gr}J_{gn} - \Omega^2 I + k_Lk_H(J_r + J_{gr} + J_{gn})\right)^2 + \Omega^6\left(\Omega^2(J_r\sqrt{E} + c_LJ_{gr}J_{gn}) - D(J_r + J_{gr} + J_{gn})\right)^2}}, \tag{A.3c}$$

where $D = c_Lk_H + c_Hk_L$, $E = (c_LJ_{gn} + c_HJ_{gr} + c_HJ_{gn})^2$, $F = (c_LJ_r + c_LJ_{gr} + c_HJ_r)^2$, $G = (J_{gr}k_H + J_{gn}k_L + J_{gn}k_H)^2$, $H = (J_rk_L + J_rk_H + J_{gr}k_L)^2$ and $I = c_Lc_HJ_r + c_Lc_HJ_{gr} + c_Lc_HJ_{gn} + J_rJ_{gr}k_H + J_rJ_{gn}k_L + J_rJ_{gn}k_H + J_{gr}J_{gn}k_L$.

$\theta_r(\Omega)$, $\theta_{gr}(\Omega)$ and $\theta_{gn}(\Omega)$ are the angular positions at rotor, gearbox and generator, respectively. c_L and c_H are the actual damping of low- and high-speed shafts.

The amplitude of angular velocity error function in the general form by using the Laplace operator S can be defined as a function of angular positions as follows

$$|e^{\omega}_{tot}(S)| = |S(\theta_r(S) - \theta_{gn}(S))|. \tag{A.4}$$

By replacing the angular positions in eq. (A.4), the result will be

$$|e^{\omega}_{tot}(S)| = \sqrt{\frac{(A_1^2|S|^6 + A_2^2|S|^4 + A_3^2|S|^2)|T_r(S)|^2 + (A_4^2|S|^6 + A_5^2|S|^4 + A_6^2|S|^2)|T_g(S)|^2}{A_7^2|S|^8 + A_8^2|S|^6 + A_9^2|S|^4 + A_{10}^2|S|^2 + A_{11}^2}}, \tag{A.5}$$

where $A_1 = J_{gr}J_{gn},\ A_2 = c_LJ_{gn} + c_HJ_{gr} + c_HJ_{gn},\ A_3 = J_{gr}k_H + J_{gn}k_L + J_{gn}k_H,\ A_4 = J_rJ_{gr},\ A_5 = c_LJ_r + c_LJ_{gr} + c_HJ_r,\ A_6 = J_rk_L + J_rk_H + J_{gr}k_L,\ A_7 = J_rJ_{gr}J_{gn},\ A_8 = c_LJ_rJ_{gn} + c_HJ_rJ_{gr} + c_LJ_{gr}J_{gn} + c_HJ_rJ_{gn},\ A_9 = c_Lc_HJ_r + c_Lc_HJ_{gr} + c_Lc_HJ_{gn} + J_rJ_{gr}k_H + J_rJ_{gn}k_L + J_rJ_{gn}k_H + J_{gr}J_{gn}k_L,\ A_{10} = c_LJ_rk_H + c_HJ_rk_L + c_LJ_{gr}k_H + c_HJ_{gr}k_L + c_LJ_{gn}k_H + c_HJ_{gn}k_L,\ A_{11} = J_rk_Lk_H + J_{gr}k_Lk_H + J_{gn}k_Lk_H.$

The denominator of angular velocity error function $e^{\omega}_{tot}(S)$ based on the described model finds the form as

$$D(e^{\omega}_{tot}(S)) = (A_7S^4 + A_8S^3 + A_9S^2 + A_{10}S + A_{11})S^2. \tag{A.6}$$

The roots of the above function are the poles of $e^{\omega}_{tot}(S)$ which belong to the set of extreme points of the response. By replacing $S = j\Omega$ for the equivalent undamped system, $D(e^{\omega}_{tot}(\Omega))$ will find the form of a complex equation. To find the roots of the resulted complex equation, the absolute value of this equation is set to be zero which turns to the following polynomial equation

$$(A_7\Omega^6 - A_9\Omega^4 + A_{11}\Omega^2)^2 + (A_{10}\Omega^3 - A_8\Omega^5)^2 = 0. \tag{A.7}$$

The above equation can be reduced to a polynomial of the order of four by the change of variable $\gamma = \Omega^2$ and eliminating the rigid modes ($\Omega = 0$), which makes it possible to find the closed form solutions of the response poles. The resulted equation is

$$A_7^2\gamma^4 + (A_8^2 - 2A_7A_9)\gamma^3 + (A_9^2 + 2A_7A_{11} - 2A_8A_{10})\gamma^2 + (A_{10}^2 - 2A_9A_{11})\gamma + A_{11}^2 = 0. \tag{A.8}$$

By assuming damping equal to zero, and considering the positiveness of γ, the two acceptable answers are obtained. The results give four values for Ω which belong to the extreme points of response. The results are two pairs of imaginary poles which the absolute value of each pair coincides with one of the system torsional eigenfrequencies described by eq. (A.1).

The results can be extended to the damped system so that also in the damped system the poles of the response coincide with the eigenfrequencies of the system, where the poles take the complex form $S = \sigma + j\omega_d = \zeta\Omega_n + j\Omega_n\sqrt{1-(\zeta)^2}$. However, the absolute value of the poles will still be $|S| = \Omega_n$.

Appendix B. Sensitivity of drivetrain system dynamic properties to the equivalent model parameters based on 3-DOF model

B1. Sensitivity of natural frequencies to the system parameters

The equations describing the sensitivity of natural frequencies to the system parameters are summarized as follows. For this case, there are two natural frequencies and five parameters which results in ten different sensitivity functions.

$$\boldsymbol{S}^{norm}_{1,1} = \frac{k_L}{2}\frac{\frac{(\frac{1}{J_{gr}}+\frac{1}{J_r})(\frac{k_H}{2J_{gn}} - \frac{k_L}{2J_r} + \frac{k_H-k_L}{2J_{gr}}) - \frac{k_H}{J_{gr}^2}}{\sqrt{(\frac{k_H}{J_{gn}} - \frac{k_L}{J_r} + \frac{k_H-k_L}{J_{gr}})^2 + \frac{4k_Lk_H}{J_{gr}^2}}} + \frac{1}{2J_{gr}} + \frac{1}{2J_r}}{\frac{k_H}{2J_{gn}} - \sqrt{(\frac{k_H}{2J_{gn}} - \frac{k_L}{2J_r} + \frac{k_H-k_L}{2J_{gr}})^2 + \frac{k_Lk_H}{J_{gr}^2}} + \frac{k_L}{2J_r} + \frac{k_H+k_L}{2J_{gr}}}, \tag{B.1}$$

$$\boldsymbol{S}^{norm}_{2,1} = \frac{k_L}{2}\frac{(\frac{1}{2J_{gr}} - \frac{(\frac{1}{J_{gr}}+\frac{1}{J_r})(\frac{k_H}{2J_{gn}} - \frac{k_L}{2J_r} + \frac{k_H-k_L}{2J_{gr}}) - \frac{k_H}{J_{gr}^2}}{\sqrt{(\frac{k_H}{J_{gn}} - \frac{k_L}{J_r} + \frac{k_H-k_L}{J_{gr}})^2 + \frac{4k_Lk_H}{J_{gr}^2}}} + \frac{1}{2J_r})}{\sqrt{(\frac{k_H}{2J_{gn}} - \frac{k_L}{2J_r} + \frac{k_H-k_L}{2J_{gr}})^2 + \frac{k_Lk_H}{J_{gr}^2}} + \frac{k_H}{2J_{gn}} + \frac{k_L}{2J_r} + \frac{k_H+k_L}{2J_{gr}}}, \tag{B.2}$$

$$\boldsymbol{S}^{norm}_{1,2} = \frac{k_H}{2}\frac{\frac{1}{2J_{gn}} - \frac{(\frac{1}{J_{gr}}+\frac{1}{J_r})(\frac{k_H}{2J_{gn}} - \frac{k_L}{2J_r} + \frac{k_H-k_L}{2J_{gr}}) + \frac{k_L}{J_{gr}^2}}{\sqrt{(\frac{k_H}{J_{gn}} - \frac{k_L}{J_r} + \frac{k_H-k_L}{J_{gr}})^2 + \frac{4k_Lk_H}{J_{gr}^2}}} + \frac{1}{2J_{gr}}}{\frac{k_H}{2J_{gn}} - \sqrt{(\frac{k_H}{2J_{gn}} - \frac{k_L}{2J_r} + \frac{k_H-k_L}{2J_{gr}})^2 + \frac{k_Lk_H}{J_{gr}^2}} + \frac{k_L}{2J_r} + \frac{k_H+k_L}{2J_{gr}}}, \tag{B.3}$$

$$\boldsymbol{S}^{norm}_{2,2} = \frac{k_H}{2}\frac{\frac{(\frac{1}{J_{gn}}+\frac{1}{J_{gr}})(\frac{k_H}{2J_{gn}} - \frac{k_L}{2J_r} + \frac{k_H-k_L}{2J_{gr}}) + \frac{k_L}{J_{gr}^2}}{\sqrt{(\frac{k_H}{J_{gn}} - \frac{k_L}{J_r} + \frac{k_H-k_L}{J_{gr}})^2 + \frac{4k_Lk_H}{J_{gr}^2}}} + \frac{1}{2J_{gn}} + \frac{1}{2J_{gr}}}{\sqrt{(\frac{k_H}{2J_{gn}} - \frac{k_L}{2J_r} + \frac{k_H-k_L}{2J_{gr}})^2 + \frac{k_Lk_H}{J_{gr}^2}} + \frac{k_H}{2J_{gn}} + \frac{k_L}{2J_r} + \frac{k_H+k_L}{2J_{gr}}}, \tag{B.4}$$

$$\boldsymbol{S}_{1,3}^{norm} = -\frac{J_r}{2}\frac{\frac{k_L}{2J_r^2} + \frac{k_L(\frac{k_H}{2J_{gn}} - \frac{k_L}{2J_r} + \frac{k_H - k_L}{2J_{gr}})}{2J_r^2\sqrt{(\frac{k_H}{2J_{gn}} - \frac{k_L}{2J_r} + \frac{k_H - k_L}{2J_{gr}})^2 + \frac{k_L k_H}{J_{gr}^2}}}}{\frac{k_H}{2J_{gn}} - \sqrt{(\frac{k_H}{2J_{gn}} - \frac{k_L}{2J_r} + \frac{k_H - k_L}{2J_{gr}})^2 + \frac{k_L k_H}{J_{gr}^2}} + \frac{k_L}{2J_r} + \frac{k_H + k_L}{2J_{gr}}}, \tag{B.5}$$

$$\boldsymbol{S}_{2,3}^{norm} = -\frac{J_r}{2}\frac{\frac{k_L}{2J_r^2} - \frac{k_L(\frac{k_H}{2J_{gn}} - \frac{k_L}{2J_r} + \frac{k_H - k_L}{2J_{gr}})}{2J_r^2\sqrt{(\frac{k_H}{2J_{gn}} - \frac{k_L}{2J_r} + \frac{k_H - k_L}{2J_{gr}})^2 + \frac{k_L k_H}{J_{gr}^2}}})}{\sqrt{(\frac{k_H}{2J_{gn}} - \frac{k_L}{2J_r} + \frac{k_H - k_L}{2J_{gr}})^2 + \frac{k_L k_H}{J_{gr}^2}} + \frac{k_H}{2J_{gn}} + \frac{k_L}{2J_r} + \frac{k_H + k_L}{2J_{gr}}}, \tag{B.6}$$

$$\boldsymbol{S}_{1,4}^{norm} = -\frac{J_{gr}}{2}\frac{\frac{k_H + k_L}{2J_{gr}^2} - \frac{\frac{2k_L k_H}{J_{gr}^3} + \frac{(k_H - k_L)(\frac{k_H}{2J_{gn}} - \frac{k_L}{2J_r} + \frac{k_H - k_L}{2J_{gr}})}{J_{gr}^2}}{2\sqrt{(\frac{k_H}{2J_{gn}} - \frac{k_L}{2J_r} + \frac{k_H - k_L}{2J_{gr}})^2 + \frac{k_L k_H}{J_{gr}^2}}}}{\frac{k_H}{2J_{gn}} - \sqrt{(\frac{k_H}{2J_{gn}} - \frac{k_L}{2J_r} + \frac{k_H - k_L}{2J_{gr}})^2 + \frac{k_L k_H}{J_{gr}^2}} + \frac{k_L}{2J_r} + \frac{k_H + k_L}{2J_{gr}}}, \tag{B.7}$$

$$\boldsymbol{S}_{2,4}^{norm} = -\frac{J_{gr}}{2}\frac{\frac{\frac{2k_L k_H}{J_{gr}^3} + \frac{(k_H - k_L)(\frac{k_H}{2J_{gn}} - \frac{k_L}{2J_r} + \frac{k_H - k_L}{2J_{gr}})}{J_{gr}^2}}{2\sqrt{(\frac{k_H}{2J_{gn}} - \frac{k_L}{2J_r} + \frac{k_H - k_L}{2J_{gr}})^2 + \frac{k_L k_H}{J_{gr}^2}}} + \frac{k_H + k_L}{2J_{gr}^2}}{\sqrt{(\frac{k_H}{2J_{gn}} - \frac{k_L}{2J_r} + \frac{k_H - k_L}{2J_{gr}})^2 + \frac{k_L k_H}{J_{gr}^2}} + \frac{k_H}{2J_{gn}} + \frac{k_L}{2J_r} + \frac{k_H + k_L}{2J_{gr}}}, \tag{B.8}$$

$$\boldsymbol{S}_{1,5}^{norm} = -\frac{J_{gn}}{2}\frac{\frac{k_H}{2J_{gn}^2} - \frac{k_H(\frac{k_H}{2J_{gn}} - \frac{k_L}{2J_r} + \frac{k_H - k_L}{2J_{gr}})}{2J_{gn}^2\sqrt{(\frac{k_H}{2J_{gn}} - \frac{k_L}{2J_r} + \frac{k_H - k_L}{2J_{gr}})^2 + \frac{k_L k_H}{J_{gr}^2}}}}{\frac{k_H}{2J_{gn}} - \sqrt{(\frac{k_H}{2J_{gn}} - \frac{k_L}{2J_r} + \frac{k_H - k_L}{2J_{gr}})^2 + \frac{k_L k_H}{J_{gr}^2}} + \frac{k_L}{2J_r} + \frac{k_H + k_L}{2J_{gr}}}, \tag{B.9}$$

$$\boldsymbol{S}_{2,5}^{norm} = -\frac{J_{gn}}{2}\frac{\frac{k_H}{2J_{gn}^2} + \frac{k_H(\frac{k_H}{2J_{gn}} - \frac{k_L}{2J_r} + \frac{k_H - k_L}{2J_{gr}})}{2J_{gn}^2\sqrt{(\frac{k_H}{2J_{gn}} - \frac{k_L}{2J_r} + \frac{k_H - k_L}{2J_{gr}})^2 + \frac{k_L k_H}{J_{gr}^2}}}}{\sqrt{(\frac{k_H}{2J_{gn}} - \frac{k_L}{2J_r} + \frac{k_H - k_L}{2J_{gr}})^2 + \frac{k_L k_H}{J_{gr}^2}} + \frac{k_H}{2J_{gn}} + \frac{k_L}{2J_r} + \frac{k_H + k_L}{2J_{gr}}}, \tag{B.10}$$

B2. Sensitivity of normal modes to the system parameters

The sensitivity of normal modes to parameters variations can be defined for each element of eigenvector associated to each eigenfrequency. Therefore, for the under consideration 3-DOF model with two nonrigid modes, and five parameters of system, thirty different sensitivity functions are derived. For instance, the sensitivity of the eigenvector element related to gearbox, due to the 1*st* and 2*nd* modes, to variations in system parameters are brought as follows:

$$\boldsymbol{S}_{5,1}^{norm} = \frac{-K_L(\frac{2K_L(K_L - J_r A + K_L(J_r(\frac{2(\frac{1}{2J_{gr}} + \frac{1}{2J_r})P - \frac{K_H}{J_{gr}^2}}{2Q} + \frac{1}{2J_{gr}} + \frac{1}{2J_r}) - 1))}{(K_L - J_r A)^3} + \frac{2J_{gn}K_H^2(\frac{2(\frac{1}{2J_{gr}} + \frac{1}{2J_r})P - \frac{K_H}{J_{gr}^2}}{2Q} + \frac{1}{2J_{gr}} + \frac{1}{2J_r})}{(K_H - J_{gn}A)^3})}{2(\frac{K_H^2}{(K_H - J_{gn}A)^2} + \frac{K_L^2}{(K_L - J_r A)^2} + 1)} \tag{B.11}$$

$$\boldsymbol{S}_{5,2}^{norm} = \frac{-K_H(\frac{2K_H(K_H - J_{gn}A + K_H(J_{gn}(\frac{1}{2J_{gn}} - \frac{2(\frac{1}{2J_{gn}} + \frac{1}{2J_{gr}})P + \frac{K_L}{J_{gr}^2}}{2Q} + \frac{1}{2J_{gr}}) - 1))}{(K_H - J_{gn}A)^3} + \frac{2J_r K_L^2(\frac{1}{2J_{gn}} - \frac{2(\frac{1}{2J_{gn}} + \frac{1}{2J_{gr}})P + \frac{K_L}{J_{gr}^2}}{2Q} + \frac{1}{2J_{gr}})}{(K_L - J_r A)^3})}{2(\frac{K_H^2}{(K_H - J_{gn}A)^2} + \frac{K_L^2}{(K_L - J_r A)^2} + 1)} \tag{B.12}$$

$$\boldsymbol{S}_{5,3}^{norm} = \frac{-J_r(\frac{2K_L^2(A - J_r(\frac{K_L}{2J_r^2} + \frac{K_L P}{2J_r^2 Q}))}{(K_L - J_r A)^3} - \frac{2J_{gn}K_H^2(\frac{K_L}{2J_r^2} + \frac{K_L P}{2J_r^2 Q})}{(K_H - J_{gn}A)^3})}{2(\frac{K_H^2}{(K_H - J_{gn}A)^2} + \frac{K_L^2}{(K_L - J_r A)^2} + 1)} \tag{B.13}$$

$$\boldsymbol{S}_{5,4}^{norm} = \frac{-J_{gr}(\frac{2J_{gn}K_H^2(\frac{\frac{2K_H K_L}{J_{gr}^3} + \frac{(K_H - K_L)P}{J_{gr}^2}}{2Q} - \frac{K_H + K_L}{2J_{gr}^2})}{(K_H - J_{gn}A)^3} + \frac{2J_r K_L^2(\frac{\frac{2K_H K_L}{J_{gr}^3} + \frac{(K_H - K_L)P}{J_{gr}^2}}{2Q} - \frac{K_H + K_L}{2J_{gr}^2})}{(K_L - J_r A)^3})}{2(\frac{K_H^2}{(K_H - J_{gn}A)^2} + \frac{K_L^2}{(K_L - J_r A)^2} + 1)} \tag{B.14}$$

$$S_{5,5}^{norm} = \frac{-J_{gn}\left(\frac{2K_H^2(A-J_{gn}(\frac{K_H}{2J_{gn}^2}-\frac{K_H P}{2J_{gn}^2 Q}))}{(K_H-J_{gn}A)^3} - \frac{2J_r K_L^2(\frac{K_H}{2J_{gn}^2}-\frac{K_H P}{2J_{gn}^2 Q})}{(K_L-J_r A)^3}\right)}{2\left(\frac{K_H^2}{(K_H-J_{gn}A)^2}+\frac{K_L^2}{(K_L-J_r A)^2}+1\right)} \tag{B.15}$$

$$S_{6,1}^{norm} = \frac{-K_L\left(\frac{2K_L(K_L-J_r B+K_L(J_r(\frac{1}{2J_{gr}}-\frac{2(\frac{1}{2J_{gr}}+\frac{1}{2J_r})P-\frac{K_H}{J_{gr}^2}}{2Q}+\frac{1}{2J_r})-1))}{(K_L-J_r B)^3} + \frac{2J_{gn}K_H^2(\frac{1}{2J_{gr}}-\frac{2(\frac{1}{2J_{gr}}+\frac{1}{2J_r})P-\frac{K_H}{J_{gr}^2}}{2Q}+\frac{1}{2J_r})}{(K_H-J_{gn}B)^3}\right)}{2\left(\frac{K_H^2}{(K_H-J_{gn}B)^2}+\frac{K_L^2}{(K_L-J_r B)^2}+1\right)} \tag{B.16}$$

$$S_{6,2}^{norm} = \frac{-K_H\left(\frac{2K_H(K_H-J_{gn}B+(K_H(J_{gn}(\frac{2(\frac{1}{2J_{gn}}+\frac{1}{2J_{gr}})P+\frac{K_L}{J_{gr}^2}}{2Q}+\frac{1}{2J_{gn}}+\frac{1}{2J_{gr}})-1)))}{(K_H-J_{gn}B)^3} + \frac{2J_r K_L^2(\frac{2(\frac{1}{2J_{gn}}+\frac{1}{2J_{gr}})P+\frac{K_L}{J_{gr}^2}}{2Q}+\frac{1}{2J_{gn}}+\frac{1}{2J_{gr}})}{(K_L-J_r B)^3}\right)}{2\left(\frac{K_H^2}{(K_H-J_{gn}B)^2}+\frac{K_L^2}{(K_L-J_r B)^2}+1\right)} \tag{B.17}$$

$$S_{6,3}^{norm} = \frac{-J_r\left(\frac{2K_L^2(B-J_r(\frac{K_L}{2J_r^2}-\frac{K_L P}{2J_r^2 Q}))}{(K_L-J_r B)^3} - \frac{2J_{gn}K_H^2(\frac{K_L}{2J_r^2}-\frac{K_L P}{2J_r^2 Q})}{(K_H-J_{gn}B)^3}\right)}{2\left(\frac{K_H^2}{(K_H-J_{gn}B)^2}+\frac{K_L^2}{(K_L-J_r B)^2}+1\right)} \tag{B.18}$$

$$S_{6,4}^{norm} = \frac{J_{gr}\left(\frac{2J_{gn}K_H^2(\frac{\frac{2K_HK_L}{J_{gr}^3}+\frac{(K_H-K_L)P}{J_{gr}^2}}{2Q}+\frac{K_H+K_L}{2J_{gr}^2})}{(K_H-J_{gn}B)^3} + \frac{2J_r K_L^2(\frac{\frac{2K_HK_L}{J_{gr}^3}+\frac{(K_H-K_L)P}{J_{gr}^2}}{2Q}+\frac{K_H+K_L}{2J_{gr}^2})}{(K_L-J_r B)^3}\right)}{2\left(\frac{K_H^2}{(K_H-J_{gn}B)^2}+\frac{K_L^2}{(K_L-J_r B)^2}+1\right)} \tag{B.19}$$

$$S_{6,5}^{norm} = \frac{-J_{gn}\left(\frac{2K_H^2(B-J_{gn}(\frac{K_H}{2J_{gn}^2}+\frac{K_H P}{2J_{gn}^2 Q}))}{(K_H-J_{gn}B)^3} - \frac{2J_r K_L^2(\frac{K_H}{2J_{gn}^2}+\frac{K_H P}{2J_{gn}^2 Q})}{(K_L-J_r B)^3}\right)}{2\left(\frac{K_H^2}{(K_H-J_{gn}B)^2}+\frac{K_L^2}{(K_L-J_r B)^2}+1\right)} \tag{B.20}$$

where
$P = \frac{K_H}{2J_{gn}} - \frac{K_L}{2J_r} + \frac{K_H-K_L}{2J_{gr}}$ and $Q = \sqrt{P^2 + \frac{K_H K_L}{J_{gr}^2}}$.

B3. Sensitivity of amplitude of response at the natural frequencies to the system parameters and loads

The sensitivity of amplitude of response at the natural frequencies to system parameters and loads can be defined for the two natural frequencies with respect to the seven system parameters and the two input/output loads which results in eighteen different cases. In the following, the closed form equations of the sensitivity analysis associated to 1*st* and 2*nd* torsional frequencies with respect to both the input and output loads are shown:

$$S_{9,8}^{norm} = \frac{T_r\sqrt{EA+G+J_{gr}^2J_{gn}^2A^2}\sqrt{A}}{2(T_g\sqrt{FA+V+J_r^2J_{gr}^2A^2}\sqrt{A}+T_r\sqrt{EA+G+J_{gr}^2J_{gn}^2A^2}\sqrt{A})} \tag{B.21}$$

$$S_{9,9}^{norm} = \frac{T_g\sqrt{FA+V+J_r^2J_{gr}^2A^2}\sqrt{A}}{2(T_g\sqrt{FA+V+J_r^2J_{gr}^2A^2}\sqrt{A}+T_r\sqrt{EA+G+J_{gr}^2J_{gn}^2A^2}\sqrt{A})} \tag{B.22}$$

$$S_{10,8}^{norm} = \frac{T_r\sqrt{EB+G+J_{gr}^2J_{gn}^2B^2}\sqrt{B}}{2(T_g\sqrt{FB+V+J_r^2J_{gr}^2B^2}\sqrt{B}+T_r\sqrt{EB+G+J_{gr}^2J_{gn}^2B^2}\sqrt{B})} \tag{B.23}$$

$$S_{10,9}^{norm} = \frac{T_g\sqrt{FB+V+J_r^2J_{gr}^2B^2}\sqrt{B}}{2(T_g\sqrt{FB+V+J_r^2J_{gr}^2B^2}\sqrt{B}+T_r\sqrt{EB+G+J_{gr}^2J_{gn}^2B^2}\sqrt{B})} \tag{B.24}$$

References

[1] A. Ioannou, A. Angus, F. Brennan, Parametric CAPEX, OPEX, and LCOE expressions for offshore wind farms based on global deployment parameters, Energy Sources, Part B: Economics, Planning, and Policy 13 (5) (2018) 281–290.
[2] S. Pfaffel, S. Faulstich, K. Rohrig, Performance and reliability of wind turbines: areview, Energies 10 (11) (2017) 1904.
[3] M. El-Kafafy, N. Gioia, P. Guillaume, J. Helsen, Long-term automatic tracking of the modal parameters of an offshore wind turbine drivetrain system in standstill condition, in: Rotating Machinery, Vibro-Acoustics & Laser Vibrometry, Vol. 7, 2019, pp. 91–99.
[4] N. Gioia, P.J. Daems, C. Peeters, P. Guillaume, J. Helsen, R. Medico, D. Deschrijver, T. Dhaene, Gaining insight in wind turbine drivetrain dynamics by means of automatic operational modal analysis combined with machine learning algorithms, in: ASME International Conference on Offshore Mechanics and Arctic Engineering Vol. 58899, 2019. p. V010T09A017

[5] M. El-Kafafy, L. Colanero, N. Gioia, C. Devriendt, P. Guillaume, J. Helsen, Modal parameters estimation of an offshore wind turbine using measured acceleration signals from the drivetrain, Struc. Health Monitoring& Damage Detection, vol. 7, pp. 41–48, 2017.
[6] F.P.G. Márquez, A.M. Tobias, J.M.P. Pérez, M. Papaelias, Condition monitoring of wind turbines: techniques and methods, Renew Energy 46 (2012) 169–178.
[7] E. Artigao, A. Honrubia-Escribano, E. Gomez-Lazaro, Current signature analysis to monitor DFIG wind turbine generators: a case study, Renew Energy 116 (2018) 5–14.
[8] S. Soua, P. Van Lieshout, A. Perera, T.H. Gan, B. Bridge, Determination of the combined vibrational and acoustic emission signature of a wind turbine gearbox and generator shaft in service as a pre-requisite for effective condition monitoring, Renew Energy 51 (2013) 175–181.
[9] W. Yang, P.J. Tavner, C.J. Crabtree, Y. Feng, Y. Qiu, Wind turbine condition monitoring: technical and commercial challenges, Wind Energy 17 (5) (2014) 673–693.
[10] O. Tonks, Q. Wang, The detection of wind turbine shaft misalignment using temperature monitoring, CIRP J. Manuf. Sci. Technol. 17 (2017) 71–79.
[11] Y. Feng, Y. Qiu, C.J. Crabtree, H. Long, P.J. Tavner, Monitoring wind turbine gearboxes, Wind Energy 16 (5) (2013) 728–740.
[12] S. Chen, M. Du, Z. Peng, Z. Feng, W. Zhang, Fault diagnosis of planetary gearbox under variable-speed conditions using an improved adaptive chirp mode decomposition, J Sound Vib 468 (2020) 115065.
[13] W. Qiao, D. Lu, A survey on wind turbine condition monitoring and fault diagnosis–part II: signals and signal processing methods, IEEE Trans. Ind. Electron. 62 (10) (2015) 6546–6557.
[14] K. Maynard, M. Trethewey, Blade and shaft crack detection using torsional vibration measurements part 3: field application demonstrations, Noise & Vibration Worldwide 32 (11) (2001) 16–23.
[15] F.K. Moghadam, A.R. Nejad, Experimental validation of angular velocity measurements for wind turbines drivetrain condition monitoring, in: Proceedings of 2*nd* International Offshore Wind Technical Conference (IOWTC) 2019, 2019. Accepted
[16] M. Suominen, J. Karhunen, A. Bekker, P. Kujala, M. Elo, H. Enlund, S. Saarinen, Full-scale measurements on board PSRV SA Agulhas II in the Baltic Sea, in: Proceedings of the International Conference on Port and Ocean Engineering Under Arctic Conditions, 2013.
[17] T.H. Patel, A.K. Darpe, Coupled bending-torsional vibration analysis of rotor with rub and crack, J Sound Vib 326 (3–5) (2009) 740–752.
[18] Z. Feng, M.J. Zuo, Fault diagnosis of planetary gearboxes via torsional vibration signal analysis, Mech Syst Signal Process 36 (2) (2013) 401–421.
[19] M.S. Lebold, K. Maynard, K. Reichard, M. Trethewey, D. Bieryla, C. Lissenden, D. Dobbins, Using torsional vibration analysis as a synergistic method for crack detection in rotating equipment, IEEE Aerospace Conf. Proc., Vol. 6 (2004) 3517–3527.
[20] S.H. Kia, H. Henao, G.A. Capolino, Torsional vibration assessment using induction machine electromagnetic torque estimation, IEEE Trans. Ind. Electron. 57 (1) (2009) 209–219.
[21] B. Lu, Y. Li, X. Wu, Z. Yang, A Review of Recent Advances in wind turbine condition monitoring and fault diagnosis, in: 2009 IEEE Power Electronics and Machines in Wind Applications, 2009, pp. 1–7.
[22] A.R. Nejad, P.F. Odgaard, T. Moan, Conceptual study of a gearbox fault detection method applied on a 5-MW spar-type floating wind turbine, Wind Energy 21 (11) (2018) 1064–1075.
[23] F.K. Moghadam, A.R. Nejad, Natural frequency estimation by using torsional response, and applications for wind turbine drivetrain fault diagnosis, Torque Conference (2020). Accepted
[24] M.S. Lebold, K. Maynard, K. Reichard, M. Trethewey, D. Bieryla, C. Lissenden, D. Dobbins, Using torsional vibration analysis as a synergistic method for crack detection in rotating equipment, IEEE Aerospace Conference Proceedings 6 (2004) 3517–3527.
[25] M. Jiang, J. Wu, X. Peng, X. Li, Nonlinearity measure based assessment method for pedestal looseness of bearing-rotor systems, J Sound Vib 411 (2017) 232–246.
[26] Y. Liu, Y. Zhao, Z.Q. Lang, J. Li, X. Yan, S. Zhao, Weighted contribution rate of nonlinear output frequency response functions and its application to rotor system fault diagnosis, J Sound Vib 460 (2019) 114882.
[27] S. Chatterton, P. Pennacchi, A. Vania, P. Rubio, Analysis of the periodic breathing of a transverse annular crack propagated in a real rotating machine, Eng Fail Anal 99 (2019) 126–140.
[28] W. Thomson, Theory of vibration with applications, CRC Press, 2018.
[29] M. Kutz, Handbook of measurements in science and engineering : Vol. 1, Wiley, Hoboken, N.J, 2013.
[30] C.J. Lissenden, S.P. Tissot, M.W. Trethewey, K.P. Maynard, Torsion response of a cracked stainless steel shaft, Fatigue Fract. Eng. Mater. Struct. 30 (8) (2007) 734–747.
[31] J. Morio, Global and local sensitivity analysis methods for a physical system, Eur. J. Phys. 32 (2011) 1577.
[32] F.K. Moghadam, A.R. Nejad, Evaluation of PMSG-based drivetrain technologies for 10 MW floating offshore wind turbines: pros and cons in a life-cycle perspective, Wind Energy (2019). Accepted
[33] A. Saltelli, S. Tarantola, K.S. Chan, A quantitative model-independent method for global sensitivity analysis of model output, Technometrics 41 (1) (1999) 39–56.
[34] F.K. Moghadam, G.F.d.S. Rebouças, A.R. Nejad, Digital twin modeling for predictive maintenance of gearboxes in floating offshore wind turbine drivetrains, Forsch Ingenieurwes (2021), doi:10.1007/s10010-021-00468-9.
[35] M. Karimirad, MARINTEK numerical tools for coupled aero-hydro-servo-elastic simulations of offshore, Wind Turbines (2019). SINTEF. MARINTEK. [Accessed, 2019]
[36] W. Rulka, SIMPACKa computer program for simulation of large-motion multibody systems, in: Multibody systems handbook, Springer, Berlin, Heidelberg, 1990, pp. 265–284.
[37] J. Licari, C.E. Ugalde-Loo, J.B. Ekanayake, N. Jenkins, Damping of torsional vibrations in a variable-speed wind turbine, IEEE Trans. Energy Convers. 28 (1) (2012) 172–180.
[38] A.K. Darpe, K. Gupta, A. Chawla, Coupled bending, longitudinal and torsional vibrations of a cracked rotor, J Sound Vib 269 (1–2) (2004) 33–60.